TRANSPORTATION RESEARCH RECORD 832

Erosion, Sedimentation, Flood Frequency, and Bridge Testing

TRANSPORTATION RESEARCH BOARD

COMMISSION ON SOCIOTECHNICAL SYSTEMS
NATIONAL RESEARCH COUNCIL

NATIONAL ACADEMY OF SCIENCES
WASHINGTON, D.C. 1981

Transportation Research Record 832
Price $5.20
Edited for TRB by Naomi Kassabian

modes
1 highway transportation
3 rail transportation
4 air transportation

subject areas
22 hydrology and hydraulics
23 environmental design
25 structures design and performance

Library of Congress Cataloging in Publication Data
National Research Council (U.S.). Transportation Research Board. Meeting.
Eorsion, sedimentation, flood frequency, and bridge testing.

(Transportation research record; 832)
Reports presented at the 60th annual meeting of the Transportation Research Board.
1. Highway engineering–addresses, essays, lectures. 2. Erosion–Addresses, essays, lectures. 3. Sedimentation and deposition–Addresses, essays, lectures. 4. Floods–Addresses, essays, lectures. 5. Bridges–Testing–Addresses, essays, lectures.
I. Title. II. Series
TE7.H5 no. 832 [TE155] 380.5s]625.7] 82-6365
ISBN 0-309-03309-8 ISSN 0361-1981 AACR2

Sponsorship of the Papers in This Transportation Research Record

GROUP 2–DESIGN AND CONSTRUCTION OF TRANSPORTATION FACILITIES
R. V. LeClerc, Washington State Department of Transportation, chairman

General Design Section
Lester A. Herr, T.Y. Lin and Associates, chairman

Committee on Hydrology, Hydraulics, and Water Quality
A. Mainard Wacker, Wyoming Highway Department, chairman
J. Sterling Jones, Federal Highway Administration, secretary
Charles J. Allen, John J. Bailey, Jr., Harry H. Barnes, Jr., Lawrence D. Bruesch, Darwin L. Christensen, Earl C. Cochran, Jr., Allen L. Cox, Richey S. Dickson, John Joseph Duffy, Rex L. Eley, Samuel V. Fox, John L. Grace, Jr., Herbert W. Gregory, Frank L. Johnson, John F. Orsborn, Clinton E. Parker, Brian M. Reich, August R. Robinson, John E. Sandahl, Martin P. Wanielista, Fred J. Watts, Henry B. Wyche, Jr.

Structures Section
LeRoy T. Oehler, Michigan Department of Transportation, chairman

Committee on Dynamics and Field Testing of Bridges
Conrad P. Heins, Jr., Univesity of Maryland, chairman
Charles F. Galambos, Federal Highway Administration, secretary
Baidar Bakht, James W. Baldwin, Jr., Furman W. Barton, William G. Byers, G.R. Cudney, Ismail A.S. Elkholy, Hota V.S. Gangarao, David William Goodpasture, Hans K. Hagemann, Celal N. Kostem, Robert H. Lee, Fred Moses, M. Noyszewski, Wallace W. Sanders, Jr., William J. Venuti, William H. Walker, Kenneth R. White, James F. Wilson

Lawrence F. Spaine, Transportation Research Board staff

Sponsorship is indicated by a footnote at the end of each report. The organizational units, officers, and members are as of December 31, 1980.

Contents

Authors of the Papers in This Record

Baldwin, J.W., Jr., College of Engineering, University of Missouri-Columbia, Columbia, MO 65211
Buchberger, Steven G., Colorado Department of Highways, 65 Clarkson, #501, Denver, CO 80218
Connelly, Gary B., Pennsylvania Department of Transportation, District 3-0, Montoursville, PA 17754
Duffield, R.C., College of Engineering, University of Missouri-Columbia, Columbia, MO 65211
Salane, H.J., College of Engineering, University of Missouri-Columbia, Columbia, MO 65211
Wyant, David C., Virginia Highway and Transportation Research Council, Box 3817, University Station, Charlottesville, VA 22903
Younkin, Larry M., Department of Civil Engineering, Bucknell University, Lewisburg, PA 17837

Prediction of Storm-Induced Sediment Yield from Highway Construction

LARRY M. YOUNKIN AND GARY B. CONNELLY

A prediction equation is presented for estimating the storm-induced increase in suspended sediment yield in a stream system due to highway construction. The equation was developed by regression analysis of data collected at nine stream-gage sites in five watersheds in Pennsylvania. Two hundred and seventy eight sets of data were included in the analysis. The equation relates factors that describe soil erodibility, rainfall, construction phases, and proximity of construction to the stream system to the increased quantity of sediment transported. The result indicates that the sediment carried by a stream increases with soil erodibility, storm-erosion index, area cleared and grubbed, cut-and-fill heights, and proximity of construction to the stream. The form of the final equation was found to be rational but the standard error of estimate was large, although not exceptional when compared with the results of other sediment-transport studies. It is concluded that the equation may be a useful tool in highway location studies, evaluation of highway development impact, and design of sediment catchment devices.

Highway construction is often cited as one of the major sources of sediment in streams. For the highway engineer and planner, a general method of predicting the increase in sediment yield in a stream system due to uncontrolled highway construction would be a useful tool for evaluating the impact of highway development. With the effect of construction and watershed parameters defined, minimum sediment yield could be a criterion applied in highway location studies. The design capacity of catchment devices in erosion-control plans could be determined and a base for evaluating the effectiveness of the plans would be available. Thus, the method would provide the capability of developing a comprehensive location and construction plan that would minimize the impact of the construction.

The quantity of soil eroded from a construction area is now usually approximated by the universal soil-loss equation (USLE) (1). This equation was originally developed by Wischmeier and Smith for agricultural lands. The applicability was broadened with the development (2) of a soil-erodibility nomograph that quantified an erodibility factor for subsoils exposed by construction. An excellent example of the employment of the USLE for estimating soil loss from a highway construction area was reported by Swerdon and Kountz (3). However, the amount of soil eroded is usually greater than that transported by the stream. The sediment yield might be related to the quantity eroded by using a delivery ratio (4), which is defined as the ratio of sediment yield to gross soil loss. But little research has been performed to evaluate this factor and it may range from 10 percent to 70 percent depending on hydrologic and watershed characteristics. Vice, Guy, and Ferguson (5) found a delivery ratio equal to 50 percent during a three-year study of sediment yield from highway construction areas in a small watershed in northern Virginia.

Younkin (6,7) attempted to develop a general sediment-yield equation from data collected during the construction of Interstate 80 through a watershed in central Pennsylvania. The equation was tested by Connelly (8) by using data obtained from a watershed in northern Pennsylvania during a period of highway construction. The equation was found to overpredict sediment yields primarily because of differences in soil erodibility and cut-and-fill work between the two studies. It was concluded that data from other projects were needed to increase the range of causative factor values to generalize a prediction equation.

This paper describes the development and application of an equation that may be employed to estimate the suspended sediment load carried by a stream system during periods of rainfall-induced erosion of disturbed soils common to highway construction. It was established by the multiple linear regression analysis of data collected during the construction of highways through five watersheds in central Pennsylvania during the period from 1968 through 1975. The variation of site conditions for the study areas has broadened the range of soil and construction factors values beyond those examined previously.

SEDIMENT-YIELD MODEL

Due to the complex nature of the erosion-transport process, it was anticipated that the relationship would be established by the multiple regression analysis of data collected from field studies. The prediction equation model was assumed to be of the following form:

$$Q_s = b_0 K^{b_1} R^{b_2} (\log A)^{b_3} b_4{}^{D} / P^{b_5} \quad (1)$$

where

Q_s = suspended sediment yield at a particular location in the stream system,
K = soil-erodibility factor,
R = storm-erosion index,
A = area of surface exposed by construction,
D = average height of cut or fill work, and
P = dimensionless proximity factor for relative location of construction to stream system.

The values of the independent factors define conditions in the watershed upstream of the particular location in the stream system. The b-constants are the regression coefficients.

FACTOR DEFINITIONS

The concept of the soil-erodibility factor K (measured in tons per acre per unit of storm-erosion index R) was taken directly from the work of Wischmeier, Johnson, and Cross (2). The K-term was employed because it is based on a great quantity of field data and is relatively easy to evaluate from information usually available to the engineer. The five soil parameters that must be known for a number of representative samples for the determination are as follows: percentage of silt, percentage of sand, organic-matter content, soil structure, and permeability. Proposed highway construction normally would be preceded by a soils and geological investigation that would yield these data.

Wischmeier and Smith (9) found that the best single rainfall variable related to soil loss is the product of the total storm rainfall energy and its maximum 30-min intensity. They define the erosion index R as follows:

$$R = (E \cdot I)/100 \quad (2)$$

where E is the energy of the storm in foot-tons per acre and I is the maximum 30-min intensity in inches

per hour. The R-value for a specific measured rainstorm may be computed by the procedure described by Wischmeier and Smith. The annual average R-value, the average time distribution of that annual value through the year, and the expected magnitudes of storm R-values for various recurrence intervals may be found in Agricultural Handbook 282 (1) for areas east of the Rocky Mountains.

Sediment yield must be a function of the area of exposed surface available to rainfall-induced erosion. For this study, the area A (in acres) was defined as that exposed by the clearing and grubbing phase of the construction. A preliminary graphical study of the data showed that Q_s best related linearly to log A on a logarithmic plot. The value of this factor may be taken from the highway plans.

Figure 1. Definition of proximity factor P.

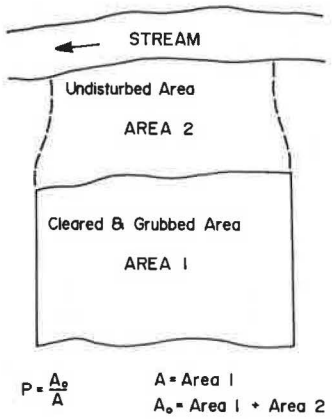

Slope length and gradient of exposed surfaces have been shown (10) to be of prime importance in the erosion process. Highway cut-and-fill slope gradients are generally standardized according to their height and it was reasoned that an average height D (in yards) of cut-and-fill work would be a measure of the slope characteristics. The average D-value of earthwork completed upstream of a particular location in a stream system may be obtained from the highway profile. The minimum value of D is zero, which occurs after clearing and grubbing have begun but before the cut-and-fill work has commenced.

The dimensionless proximity factor P was rationalized as an excellent measure of the location of the construction relative to the stream system. It was defined as follows:

$$P = A_0/A \quad (3)$$

where A_0 is the surface area (in acres) between the upslope side of the construction and the stream system as shown in Figure 1. The value of A_0 may be found by planimetering highway location maps. The minimum value of P is one that occurs when a stream passes through the construction area and sediment discharges directly into it without flowing over undisturbed surfaces.

Finally, Q_s is the highway-construction-related, suspended sediment yield (in tons) caused by rainfall.

Figure 2. Locations of field-study areas.

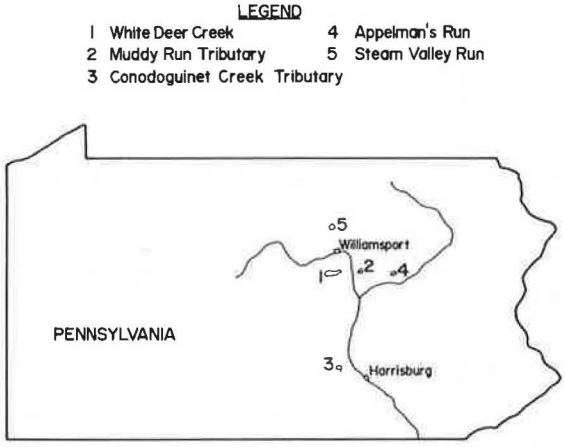

FIELD STUDIES

The five watersheds that provided the data for the development of the highway sediment yield equation were located in central Pennsylvania as shown in Figure 2. White Deer Creek is located approximately 20 miles south of Williamsport and 70 miles north of Harrisburg. It is a tributary that flows from west to east to the west branch of the Susquehanna River. Muddy Run is in the same vicinity but flows into the west branch from the east. Conodoguinet Creek flows into the Susquehanna River near Harrisburg; its watershed is located approximately 10 miles west of the city. Appelman's Run is a tributary to Fishing Creek, which flows into the north branch of the Susquehanna at Bloomsburg. Steam Valley Run flows into Blockhouse Creek, which is a tributary of Pine Creek and the west branch of the Susquehanna. It is located about 20 miles north of Williamsport. The

Table 1. Watershed characteristics.

Watershed	Area (miles^2)	Stream Slope (%)	Avg Land Slope (%)	Land Use	Mean Annual Temperature (F°)	Mean Annual Precipitation (in)	Soil	
							Overburden	Bedrock
White Deer Creek			25	Forest	50	41.7	Coarse-graded alluvium	Clinton shale
S2	29.6	1.0						
S4	4.9	2.8						
S5	3.3	3.1						
S9	1.6	6.7						
S10	2.1	6.1						
Muddy Run tributary	1.6	1.8	7	Grass and cropland	50	41.7	Fine-graded alluvium	Bloomsburg shale
Conodoguinet Creek tributary	0.8	2.0	30	Forest and grassland	53	43.4	Stony to gravelly silt loam	Clinton and Martinsburg shales
Appelman's Run	7.2	1.0	10	Grass and cropland	50	38.5	Silty clay loam	Keyser, Tonoloway, and Wills Creek shales
Steam Valley Run	5.3	5.2	20	Forest	46	35.0	Glacial till	Catskill sandstone

watersheds have similar climatic conditions but other characteristics such as areas, slopes, soils, and land uses varied as listed in Table 1. Data were collected at five locations--S2, S4, S5, S9, and S10--in the White Deer Creek stream system to provide a greater variation in construction-factor values.

The highway construction in every case was for completely new roadway locations. It was for four-lane limited-access highways in the White Deer Creek watershed for I-80, in the Conodoguinet Creek tributary watershed for I-81, and part of the work in the Muddy Run tributary watershed for state route 147. The other construction projects were for two-lane roadways. The highway or route, length, and erosion-control practice for the project in each watershed are shown in Table 2. As seen, erosion-control practices varied for the projects, and the timing of the application of the particular practice with the construction also was different. Most of the cut-and-fill work was completed at White Deer by August 1969 but the permanent seeding and mulching were not completed until the summer of 1970. At Muddy Run, earthwork was completed in the spring and the seeding and mulching were completed in the summer. The Conodoguinet Creek tributary watershed was part of a research project and the seeding and mulching were purposely not applied until the paving had been finished. In the other two watersheds, additional structural devices were employed. Reed (11) found that check dams, straw bales, and small sediment ponds may only have trap efficiencies of 5 percent, and their effect on the data for this study was ignored. The seeding and mulching kept pace with the earthwork for those two projects.

Sediment yield was measured in the White Deer Creek and the Muddy Run tributary by manual sampling supplemented by using results from several automatic samplers. It was primarily measured at the stream stations in the other stream systems by using automatic samplers supplemented by using a manual sampling. Natural sediment transport was measured upstream of construction in the White Deer Creek, Muddy Run tributary, and Appelman's Run. It was established in the Conodoguinet Creek tributary from the results of sampling for three years before construction began. Total sediment yields at stations downstream of construction were adjusted for natural transport. Vice, Guy, and Ferguson (5) adjusted their sediment-yield data for seeding and mulching. They assumed that sediment yield was reduced 50 percent on application and further reduced to 80 percent as a fairly well-established sod cover developed. It was assumed that this reduction occurred over a period of 60 days. Sterniak (12) developed a method for computing a planting factor that may be divided into measured sediment yield to adjust to unplanted conditions. The value of the planting factor varied from 1.00 before seeding and mulching to 0.20 60 days after completion of this work. The sediment data for this study were adjusted with the planting factor.

The range of factor values that occurred upstream of each of the locations in the stream systems is shown in Table 3. An average soil-erodibility factor value was established for each construction area. It was assumed that these values remained constant for the entire construction period. The storms that were included consisted exclusively of rainfall and generally occurred between March and November. Storms separated by less than 24 h were considered one event, whereas those separated by between 24 and 48 h were excluded. The minimum values for exposed area were larger than desirable to fully describe the possible range of values of that variable. But they measured the conditions when a first significant storm occurred on each watershed following the initiation of construction. The minimum value of the average height of cut-and-fill work for most of the study areas (D = 0.00) shows that measured storms had occurred before earthwork began in those areas. A proximity-factor

Table 2. Highway or route, highway length, and erosion-control practice.

Watershed	Highway or Route	Highway Length (miles)		Erosion-Control Practice
		Two-Lane	Four-Lane	
White Deer Creek	I-80			Seeding and mulching
S2		-	5.4	
S4		-	3.4	
S5		-	1.8	
S9		-	0.7	
S10		-	0.6	
Muddy Run tributary	PA-147	-	0.6	Seeding and mulching
	PA-405	1.4	-	
Conodoguinet Creek tributary	I-81	-	0.6	Seeding and mulching
Appelman's Run	PA-487	0.6	-	Check dams, seeding and mulching
Steam Valley Run	US-15	2.7	-	Check dams, straw bales, sediment ponds, seeding and mulching

Table 3. Hydrologic, soil-erodibility, construction, and location-factor data.

Watershed	Number of Storms	Range of Storm R (foot-tons per acre x inches per hour)		Avg K	Range of Area Exposed A (acres)		Range of Height of Cuts and Fills D (yd)		Range of Proximity Factor P		Construction Period
		Maximum	Minimum		Maximum	Minimum	Maximum	Minimum	Maximum	Minimum	
White Deer Creek											1968-1970
S2	28	24.0	0.3	0.15	168.8	89.9	2.55	0.00	4.27	2.15	
S4	28	26.0	0.3	0.13	110.9	47.0	2.22	0.00	5.10	2.16	
S5	28	29.2	0.3	0.15	59.6	20.3	2.14	0.00	3.22	1.09	
S9	28	27.1	0.3	0.20	14.5	9.7	2.70	0.00	1.00	1.00	
S10	28	27.1	0.3	0.14	6.0	4.1	1.90	0.00	1.00	1.00	
Muddy Run tributary	14	21.4	0.4	0.25	66.5	29.0	2.17	0.00	1.92	1.75	1969-1971
Conodoguinet Creek tributary	53	75.8	0.6	0.18	25.0	25.0	2.63	0.20	1.00	1.00	1972-1974
Appelman's Run	42	12.4	0.5	0.48	10.9	9.5	7.21	1.18	1.00	1.00	1971-1974
Steam Valley Run	29	50.3	0.5	0.21	72.4	8.8	9.04	0.00	1.32	1.00	1972-1975

value of 1.00 indicates that four of the nine locations received sediment by surface runoff over disturbed surfaces that flowed directly into the stream rather than having an undisturbed surface between construction and stream system.

REGRESSION ANALYSIS

Multiple linear regression is commonly employed to obtain a relationship between a dependent variable and an independent variable from sets of observations. The particular method employed for this study was a computerized analysis developed by Ryan, Joiner, and Ryan (13) called Minitab. The procedure was to compute a sequence of multiple linear regression equations in a stepwise manner. In the initial step, the regression equation that relates the dependent variable to one independent variable was computed. For each succeeding step, one new variable was added to the equation and the result computed; the process continued until all independent variables had been considered. The resulting equation from each step was the least-squares best-fit solution of the relationship between the dependent and the included independent variables.

Graphical studies of the data revealed that better linear relationships occurred with logarithmic plots as compared with arithmetic plots. The regression analysis was therefore performed by using the transformation of the model equation, which is given below:

$$\log Q_s = \log b_0 + b_1 \log K + b_2 \log R + b_3 \log(\log A) + D \log b_4 + b_5 \log P \quad (4)$$

The first step of the analysis entered R as the best-related independent variable and resulted in an equation that had a standard error of 0.57 and a correlation coefficient of 0.67. The second step added D and yielded a relationship that had a standard error of 0.49 and a correlation coefficient of 0.78. The equation from the third step, which addded logA, had a standard error of 0.42 and a correlation coefficient of 0.84. The next step added K and the equation had a standard error of 0.38 and a correlation coefficient of 0.87. The final step added P and resulted in an equation that had a standard error of 0.36 and a correlation coefficient of 0.89.

The solution from the final step was transformed back to the form of the original model equation and the regression coefficients were rounded off, which yielded the following equation:

$$Q_s = [4.25\, K^{1.47}\, R^{1.15}\, (\log A)^{2.71}\, 1.19^{D}]/P^{0.72} \quad (5)$$

This equation is the prediction equation for increased suspended-sediment yield in a stream system due to rainfall-induced erosion of soil from highway construction areas. It predicts the effects of soil erodibility, rainfall, size of disturbed area, slope conditions on that area, and proximity of construction to the stream.

RELIABILITY OF EQUATION

Three criteria were used to judge the effectiveness of the prediction equation. First, the signs of the regression coefficients should be in accord with physical principles. In other words, the result should satisfy the desire for a rational form. The equation passed this test. It would predict an increase in sediment yield with increases in soil erodibility, storm-erosion index, construction area exposed, and average height of cut-and-fill work. It also predicts that sediment yield would decrease as the proximity factor increases.

The second criterion, the standard error of estimate, which measures the agreement between predicted and observed values of sediment yield, was noted above in terms of the logarithmically transformed data. The standard errors (in percentages) based on the final form of the prediction equation were found to be +127 and -56. This means that about two-thirds of the measured sediment-yield values fall within the range of +127 percent and -56 percent of the predicted values from the equation. Although this is a large range of error, it is not exceptional when compared with other sediment-transport prediction methods (14). The degree of confidence placed in the results from the use of the equation should be based on this measure of reliability.

Finally, the correlation coefficient, which measures the proportion of the variation in the dependent variable that can be explained by the variation in the independent variables, was noted above to be equal to 0.89 for the final form of the equation. This result is quite good, which indicates that the general form of the equation does fit the relationship well.

It may also be noted that the range of factor values found in this study should be adequate to include most conditions met in applying the prediction equation. Care must be taken in attempting to extrapolate the equation to situations that fall outside the range of factor values that were measured in these projects.

APPLICATION OF SEDIMENT-YIELD EQUATION

Because of the dynamic construction process, the factor values would change rapidly through the construction progress. Unlike applications of the USLE to agricultural cases in which many of the factors remain constant and seasonal changes are related to a cropping-management factor, all the highway sediment-yield factors may change in relatively short time periods. The size of the area cleared and grubbed usually changes significantly in a matter of days. The proximity factor may change as the size of the area cleared increases, depending on its location relative to the stream. Earthwork generally progresses at a slower pace but would usually be completed in one construction season. As the work progresses, different subsoils may be exposed, which causes changes in the average K-value for the area. A storm with any magnitude of R could occur at any time in the process.

An estimate of the sediment yield at a point in a stream system from a particular storm may be accomplished by a straightforward application of the prediction equation. It would require the evaluation of the K-, A-, D-, and P-factors for the construction site and the calculation of the R-value from rain-gage data for the storm.

For planning and design functions, estimates must be made in probabilistic terms because of the nature of the rainfall. Estimates of the average annual sediment yield from a proposed highway project may be made by phasing estimates of construction progress quantified by using the changing values of the soil and construction factors with respect to time with average values of storm R through the same period. These latter values may be estimated from data presented in Agriculture Handbook 282 (1), which gives an isoerodent map of average annual erosion index values and the erosion-index distribution curves, an example of which is shown in Figure 3. Since the prediction equation does not relate Q_s to R linearly, estimates should be made of sediment yield by using weekly or semiweekly values of R, which approximate individual storm values,

Figure 3. Erosion-index variation.

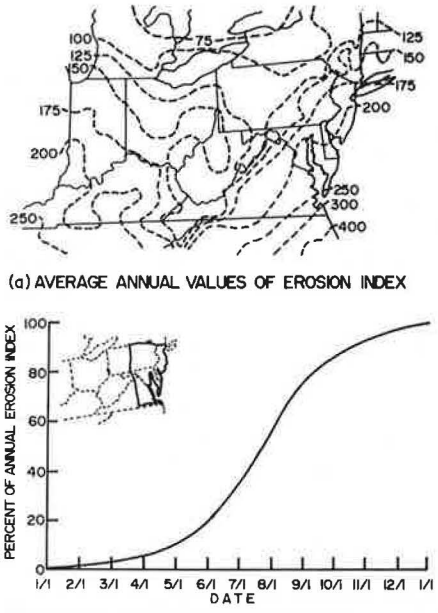

determined from the above sources. Handbook 282 also lists 5, 20, and 50 percent probability values of annual R, which could be employed in a similar fashion to estimate those probability values of annual sediment yield from construction. With this method, the timing of critical construction phases could be scheduled to occur during periods of average lower R-values.

The capacity of an erosion-control device could be established from an estimate of the sediment yield from the area being controlled. In this case, the critical combination of soil and construction factor values for the area would be substituted along with the design storm R-value into the prediction equation. Handbook 282 lists expected magnitudes of single-storm erosion-index values for frequencies of 1, 2, 5, 10, and 20 years for many locations east of the Rocky Mountains. A design storm period of two years would seem reasonable given that these devices are temporary and the low probability that the design storm would occur when the other factor values are in a critical combination condition.

CONCLUSIONS

This study has been conducted with the objective of developing an equation for predicting suspended-sediment yields in stream systems during periods of rainfall-induced erosion of disturbed soils common to uncontrolled highway construction. Factors that quantify soil erodibility, rainfall, construction phases, and relative highway location effects have been either adopted from the literature or developed for the study. A regression equation (Equation 5) was derived from 278 sets of values of these factors, which were computed from data collected in five watersheds.

The general form of the equation satisfies rational relationships. Sediment yield increases with soil erodibility, storm-erosion index, size of area cleared and grubbed, and average height of cut-and-fill work. It decreases with an increasing proximity factor. Since D is an exponent, the equation predicts sediment yield from a cleared area before earthwork has begun.

The reliability of the prediction is indicated by the standard errors of the estimate. They were found to be +127 and -56 percent. This large range is far from satisfactory but not unusual in sediment-transport studies. Results from applications of the equation should be interpreted as estimates rather than as accurate predictions. In addition, the correlation coefficient of 0.89 for the assumed linear relationship between the logarithmically transformed data indicated that the assumption was reasonable. It is also concluded that adequate ranges of values of the factors were obtained from the five watersheds to permit the equation to be applied to most highway construction sites, and extrapolation outside these ranges is not recommended.

The results of this study should be of great value to the highway engineer. By application of the prediction equation, the location of a proposed highway may be established for minimum sediment yield. Increasing the distance from a stream increases P and hence would tend to decrease Q_s. But D would then usually tend to increase due to steeper terrain and hence Q_s would tend to increase. An optimum location, from the aspect of sediment yield, could be found.

Highway construction has often been blamed for excessive increases in sediment in adjacent streams, but methods have not been readily available to quantitatively evaluate this accusation. The prediction equation may be employed to estimate the quantity of sediment carried by a stream as a result of a particular storm on construction-site conditions at the time. It may also be used to estimate the total yield produced over the life of the project. In addition, highway construction often occurs in connection with the construction of housing developments, shopping centers, industrial parks, and other kinds of urban expansion. This equation may be employed to estimate the portion of the sediment yield due to highway construction.

This study was conducted by using data that generally showed little effect from erosion and sediment-control measures. The result may thus be used as a basis for comparison to evaluate the effectiveness of control methods. The equation may also be employed to determine the design capacity for catchment devices.

ACKNOWLEDGMENT

The data from White Deer Creek and the Muddy Run tributary and the general model development were part of a research project conducted by Bucknell University under the sponsorship of the Pennsylvania Department of Transportation (PennDOT) and the Federal Highway Administration (FHWA). It was coordinated by William G. Weber and Foster C. Sankey of PennDOT. The data from the Conodoguinet Creek tributary, Appelman's Run, and Stream Valley Run were collected by the U.S. Geological Survey (USGS) under the sponsorship of PennDOT and the Pennsylvania Department of Environmental Resources, USGS, and FHWA. They were provided by Lloyd Reed of the USGS. Much of the soil and construction phase data were obtained from PennDOT files.

REFERENCES

1. W.H. Wischmeier and D.D. Smith. Rainfall Erosion Losses from Croplands East of the Rocky Mountains. Agricultural Research Service, U.S. Department of Agriculture Handbook 282, 1965, 47 pp.
2. W.H. Wischmeier, C.B. Johnson, and B.V. Cross.

A Soil Erodibility Nomograph for Farmland and Construction Sites. Journal of Soil and Water Conservation, Vol. 26, 1971, pp. 189-193.
3. P.M. Swerdon and R.R. Kountz. Sediment Runoff Control at Highway Construction Sites. Pennsylvania State Univ., University Park, PA, Engineering Res. Bull. B-108, 1973, 120 pp.
4. Guidelines for the Control of Erosion and Sediment in Urban Areas of the Northeast. Soil Conservation Service, U.S. Department of Agriculture, Upper Darby, PA, 1970, 88 pp.
5. R.B. Vice, H.P. Guy, and G.E. Ferguson. Sediment Movement in an Area of Suburban Highway Construction, Scott Run Basin, Fairfax County, Virginia, 1961-1964. U.S. Geological Survey, Water Supply Paper 1951-E, 1969.
6. L.M. Younkin. Effects of Highway Construction on Sediment Loads in Streams. In Soil Erosion: Causes and Mechanisms; Prevention and Control. HRB, Special Rept. 135, 1973, pp. 82-93.
7. L.M. Younkin. Prediction of the Increase in Suspended Sediment Transport Due to Highway Construction. Bucknell Univ., Lewisburg, PA, Civil Engineering Res. Rept. 74-2, 1974, 126 pp.
8. G.B. Connelly. An Analysis of Suspended Sediment Transport in Steam Valley Run due to Highway Construction. Bucknell Univ., Lewisburg, PA, M.S. thesis, 1978, 84 pp.
9. W.H. Wischmeier and D.D. Smith. Rainfall Energy and Its Relationship to Soil Loss. Transactions of the American Geological Union, Vol. 39, 1958, pp. 285-291.
10. A.W. Zingg. Degree and Length of Land Slope as It Affects Soil Loss in Runoff. Agricultural Engineering, Vol. 21, 1940, pp. 59-64.
11. L.A. Reed. Effectiveness of Sediment-Control Techniques Used During Highway Construction in Central Pennsylvania. U.S. Geological Survey, Open-File Rept. 77-498, 1977, 79 pp.
12. R.S. Sterniak. An Analysis of Storm Turbidigraphs Affected by Highway Construction. Bucknell Univ., Lewisburg, PA, M.S. thesis, 1973, 87 pp.
13. T.A. Ryan, B.L. Joiner, and B.F. Ryan. Minitab, Student Handbook. Duxburg Press, North Scituate, MA, 1976, 162 pp.
14. American Society of Civil Engineers. Sedimentation Engineering. ASCE, New York, NY, Manuals and Reports on Engineering Practice 54, 1975, 745 pp.

Publication of this paper sponsored by Committee on Hydrology, Hydraulics, and Water Quality.

Evaluation of Filter Fabrics for Use in Silt Fences

DAVID C. WYANT

This study was conducted to develop tests that simulate field conditions and that could be used to generate information for the formulation of specifications for purchasing filter fabrics to be used to construct silt fences. Fifteen fabrics were subjected to seven tests devised to evaluate their performance. Two of the tests—laboratory filtering efficiency and warp tensile strength—have been adopted by the Virginia Department of Highways and Transportation for evaluating filter fabrics to be used on construction projects. Three of the four parameters found to be critical in the design of a silt fence—filtering efficiency, flow rate, and warp tensile strength—are ascertained by these two tests. A third test, to determine the fourth critical parameter (resistance to damage by ultraviolet rays), is reported but was not recommended to the department for use because of its lack of reproducibility. Further work on a method for evaluating this critical parameter is needed.

Because accelerated erosion can result from areas denuded during highway construction, the policy of the Virginia Department of Highways and Transportation is to employ protective measures on all projects and to establish vegetation as early as possible. In addition to vegetation, nonvegetative temporary erosion and sediment-control measures are needed to prevent the construction-generated silt from being carried into nearby waterways or onto adjoining properties. These nonvegetative measures are especially useful for the retention of silt before vegetation is established.

The department uses various types of nonvegetative-control measures to impede the flow of sediment-laden waters and to filter out sediment. The most commonly used measures are barriers made of straw, gravel or crushed stone, and brush. In very critical areas, however, the protection provided by these barriers has not been sufficient. Faced with this problem and recognizing that a large number of fabrics had been introduced to the highway industry for use as filter materials, in 1975 the department put into effect a special provision that allowed contractors to use fabrics to construct silt fences.

Different fabric manufacturers produce materials of different properties and use the results of different approval tests, such as those sanctioned by the American Society for Testing and Materials (ASTM) (1), as evidence of their quality. Also, the properties of the materials do not clearly relate to the properties desired of a fabric to be incorporated in a silt fence. Therefore, a study was initiated to develop tests that could be used to evaluate the properties of the fabrics and provide information that might aid in the development of specifications to be stipulated in purchasing them (2).

OBJECTIVE

The objective of the study was to develop information for the formulation of specifications for use in purchasing filter fabrics for building silt fences on highway construction projects. To achieve this objective, the performance desired of an installed silt fence made of fabric had to be established along with a valid estimation of what is reasonably achievable. Therefore, the first objective was to develop tests that closely simulated the conditions to which a silt fence is exposed. In addition, the tests were to be of a type that could be performed without any large investment in additional testing equipment.

CRITERIA FOR TESTS AND FABRICS

In developing the evaluative tests, it was decided that they should simulate field conditions. The criteria established for the fabrics were that they must have the following properties:

1. Sufficient strength to resist the force of the sediment-laden water without excessive elongation,
2. Resistance to the effects of ultraviolet rays from the sun,
3. Resistance to the effects of water of low or high pH, and
4. Ability to filter out most of the soil carried in the runoff from a construction project without unduly impeding the flow.

During the course of the testing program, it was decided that the effects of permeability would be investigated along with the susceptibility of the fabrics to creep.

FABRICS TESTED

Fifteen fabrics were received from their manufacturers for testing. Table 1 lists the fabrics and their manufacturers.

Table 1. Fabrics tested.

Trade Name	Manufacturer or Distributor
Bidim C-22	Monsanto Textiles Co.
Filter-X	Carthage Mills
Polyfilter X	
Polyfilter GB	
Laurel Erosion Cloth, types I and II	Advance Construction Specialties Co.
Polyfelt TS-200, TS-300, and TS-400	
Mirafi 140	Celanese Fibers Marketing Corp.
Monofelt	Menardi Southern Division, United States Filter Corp.
Monofilter	
Supac 5-E (PR165A)	Phillips Fibers Corp.
Supac 4-P	
Typar 3401	E.I. DuPont de Nemours and Co., Inc.

DISCUSSION OF RESULTS

Seven tests were developed for evaluating the fabrics. The data obtained from two of the tests--water permeability and field filtering efficiency--indicated no trends and are not reproducible. Therefore, they were not considered for further use and are not discussed in this paper. The test for determining the effects of pH indicated no adverse effects from exposure to solutions that cover the extremes of pH encountered in the field; thus this test is not useful. A fourth test, that for creep, also proved not to be useful.

The remaining tests--those for filtering efficiency and flow rate, tensile strength, and resistance to damage by ultraviolet rays--are discussed in the following sections.

Laboratory Filtering Efficiency and Flow Rate

In Virginia, each of the three dominant soil types is linked to one of the three major geological provinces. Clayey soils overlie limestone bedrock in the Valley and Ridge Province of western Virginia; silty soils overlie mica-rich granite in the Piedmont area; and sandy materials overlie the relatively young sediments in the Coastal Plain Province. A large sample of each of these soils was collected, dried, and sieved. The gradation curves are given in Figure 1.

Since straw-bale barriers are considered the standard control measure used by the department, it was decided to evaluate the filter fabrics under conditions to which straw-bale barriers are subjected. It was known from previous work, however, that filter fabrics acted more like a dam than did straw bales (3) and that they therefore could not be subjected to high flow rates. Consequently, it was decided to test the fabrics in the laboratory in a flume that had a slope of 8 percent, the slope of the average ditch in which straw bales are installed. To simulate runoff water, a sediment-laden mixture of 3000 ppm was selected, since the previous work had shown that this suspended-solids value was the maximum encountered in the field during a noncatastrophic storm event. Three such mixtures were run through each fabric to determine the effect three storm events would have on the filtering capability and flow rate. It had been found that, usually, after three storm events of greater than

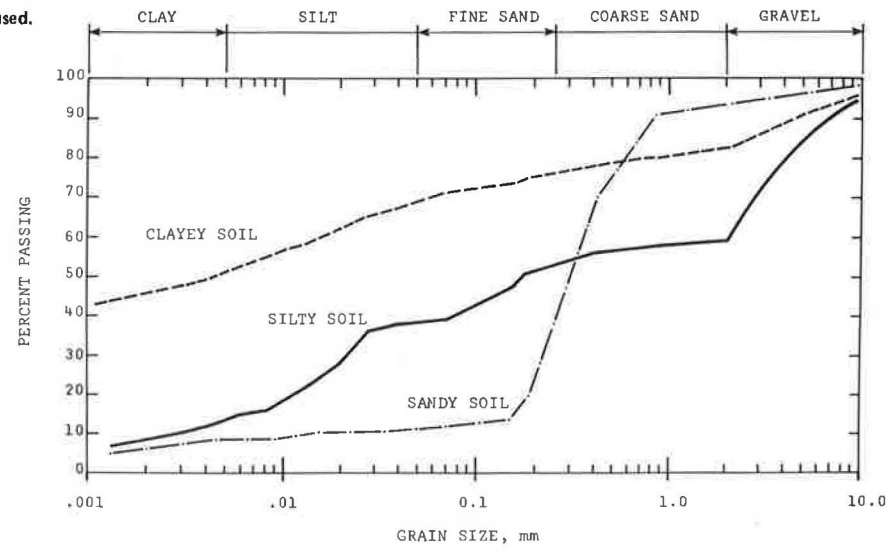

Figure 1. Gradation curves for three soils used.

0.5 in of rainfall, silt fences were inoperable unless they were cleaned out.

Three samples of each fabric were evaluated by using each of the three soils. Sediment-laden water was generated for each test by adding 150 g of minus-10 material to 50 L of uncontaminated water. Relatively clean stream water was transported to the laboratory, since tap water supplied by the local municipality contains alum, a coagulant. The alum will settle out particles quicker than will stream water and thus indicate a filtering efficiency and flow rate higher than would be found in the field.

Each soil was sieved on the No. 10 screen to obtain particles that had 2.00-mm maximum size because it was believed that particles larger than that would not be in suspension in the field. The above assumption seems to be reasonable, since soil particles 2.00 mm large would settle 1 m in less than 10 s in still water (4).

The soil and water were thoroughly mixed, the resultant mixture was poured immediately behind the fabric sample into the flume, a clock was started, and the time required to filter 50 L of the sediment-laden water was recorded. The filtered water was collected in a container and a representative, depth-integrated, well-mixed sample of the filtrate was obtained. The suspended-solids level of the filtrate was determined following the procedure for nonfiltrable residue described in the 14th edition of Standard Methods for the Examination of Water and Wastewater (5). The filtering efficiency (FE) of the fabric was calculated as follows:

$$FE\ (\text{percent}) = [(SS_{before} - SS_{after})/SS_{before}] \times 100.$$

SS_{before} and SS_{after} are the suspended-solids values before and after filtering, respectively.

By using the filtering efficiency determined and the corresponding gradation curve of the soil (Figure 1), the largest particle that passed through the fabric was determined. The flow rate was determined for this standard-size sample from the known volume of 50 L and the time required for filtration.

Table 2 gives the results of the laboratory filtration tests. The flow rate, the filtering efficiency, and the largest particle size of the soil that passed through each fabric are indicated. As shown, the results varied considerably among soil types as well as within each type.

For the sandy soil, a clay-sized particle was the largest that passed through the fabrics. Polyfilter GB and Polyfilter X fabrics allowed the larger clay particles (0.004 mm) to pass through, whereas the other fabrics filtered down to the smallest clay particle (0.001 mm) measured in the study. The results for filtering efficiency on this soil were high (greater than 92 percent), which should be expected when most of the particles dropped out of suspension very quickly. Figure 1 indicates that approximately 85 percent of the particles are larger than 0.15 mm and these particles take 67 s to settle 1 m in still water (4). Since only approximately 15 percent of the particles of this sandy soil (Figure 1) were in suspension after 1 min, very little clogging of the fabric openings occurred, even during the three storm events simulated for each fabric sample.

The flow rate varied from a low of 0.01 gal/ft²/ min (Typar 3401) to a high of 86.0 gal/ft²/ min (Laurel Erosion Cloth II). In Table 2 there seem to be no definite trends among the three columns of results for the sandy soil. The filtering efficiency and largest particle to pass through the fabric did not vary as much as the flow rates did.

As indicated in Table 2, most of the largest particles that passed through the fabrics were in the clay size range (less than 0.005 mm) and in still water take more than 7 h to settle 1 m (4). Since the water retained behind a silt fence is not completely still and the fence is not higher than 3 ft, the settlement of these particles would require that the fence perform more like a dam than like a filtering device. However, because of the high volume of water that usually accumulates behind a silt fence, it would be impossible for the fence to act like a dam without structural failures or the sediment-laden water going around or over it. In addition, clay particles have electrical charges on their surfaces that may keep them in motion (Brownian movement) and thus prevent them from settling. Consequently, with a silt fence it would seem best to attempt to retain the silt-sized particles. As indicated earlier, the smallest silt-sized particle (0.005 mm) would take more than 7 h to settle out in still water.

Table 2. Laboratory-filtration-test results.

Material	Sandy Soil			Silty Soil			Clayey Soil		
	Flow Rate (gal/ft²/min)	Filtering Efficiency (%)	Particle Size[a] (mm)	Flow Rate (gal/ft²/min)	Filtering Efficiency (%)	Particle Size[a] (mm)	Flow Rate (gal/ft²/min)	Filtering Efficiency (%)	Particle Size[a] (mm)
Bidim C-22 (NW)	1.7	97	0.001	0.2	95	0.001	0.6	97	0.001
Filter-X (NW)	0.2	98	0.001	0.2	98	0.001	0.6	94	0.001
Laurel Erosion Cloth type I (W)	0.4	97	0.001	0.1	99	0.001	0.3	98	0.001
Laurel Erosion Cloth type II (W)	86.0	94	0.001	59.9	49	0.180	63.5	85	0.001
Mirafi 140 (NW)	0.4	98	0.001	0.2	98	0.001	0.2	99	0.001
Monofelt (NW)	0.4	99	0.001	0.3	90	0.001	0.3	99	0.001
Monofilter (W)	0.2	98	0.001	0.1	94	0.001	0.2	95	0.001
Polyfelt TS-200 (NW)	3.8	97	0.001	0.2	99	0.001	1.1	94	0.001
Polyfelt TS-300 (NW)	2.2	97	0.001	0.3	99	0.001	0.03	93	0.001
Polyfelt TS-400 (NW)	2.7	98	0.001	0.5	99	0.001	0.2	95	0.001
Polyfilter GB (W)	53.4	92	0.004	5.3	84	0.008	3.1	88	0.001
Polyfilter X (W)	5.1	92	0.004	0.4	88	0.004	0.5	89	0.001
Supac 5-E (PR165A) (NW)	0.2	99	0.001	0.3	98	0.001	0.2	98	0.001
Supac 4-P (NW)	0.1	99	0.001	0.002	100	0.001	0.2	98	0.001
Typar 3401 (NW)	0.01	99	0.001	0.1	94	0.001	0.2	97	0.001

Note: W = woven; NW = nonwoven.
[a]Largest particle that passes through fabric.

In light of the settling times mentioned above, most of the suspended particles to be filtered will be in the silt and fine-sand particle ranges. Of the three soils used in the study, the silty soil from the Piedmont region has the highest percentage (40 percent) of these particles, as shown below:

Grain Size Range	Soil Type		
	Clayey	Silty	Sandy
Clay	51	13	8
Silt	19	26	2
Fine sand	7	14	30
Coarse sand	5	7	54
Gravel	18	40	6

In addition, Figure 1 shows that the gradation curve for the silty soil is more uniform than are the curves for the other two soils.

The filtration-test results for the silty soil are more varied than are those for the clayey and the sandy soils. At flow rates from 0.002 to 59.90 gal/ft²/min, the filtering efficiencies range from 49 to 100 percent and the particle sizes from 0.001 mm (clay) to 0.180 mm (fine sand). The rates for the three woven fabrics (Laurel Erosion Cloth II, Polyfilter GB, and Polyfilter X), although quite different (from 0.4 to 59.9 gal/ft²/min), allowed the largest particle to pass through. However, with the exception of the first two of these, all the fabrics retained soil particles larger than clay size.

The results for the clayey soil indicate that only clay-sized particles passed through the fabrics. However, the removal of soil particles was greater than 90 percent for all the fabrics except the three just named. The flow rate was high for Laurel Erosion Cloth II (63.5 gal/ft²/min), whereas Polyfilter GB and Polyfilter X had flow rates (3.1 and 0.5 gal/ft²/min, respectively) similar to those of the other fabrics. Most of the flow rates were between 0.2 and 0.6 gal/ft²/min. Since the most erodible soil in Virginia is the micaceous silty soil in the Piedmont (1.2-4.3 tons/acre/year of soil loss in undisturbed areas) (6), it should be used in evaluating fabrics.

Strength

Silt fences need sufficient tensile strength to withstand the forces exerted by the storm runoff and collected silt. Fabric strength also becomes important with certain modifications in installation practices (7), such as the elimination of the reinforcing wire and the reduction in supports. These modifications would simplify the installation of silt fences and thus reduce the cost. When these modifications are considered, equally as important as the tensile strength and selection of the fabric is the elongation, or strain. Silt fences without reinforcing wire and with the maximum allowed support spacing of 10.0 ft cannot function properly with more than 20 percent elongation. At this elongation, they would sag more than 3.0 in between posts. Therefore, the strength at 20 percent elongation is very important.

Several factors considered in the tensile testing are discussed below.

Rate of Strain

In testing soils, a very slow rate of strain of 1-2 percent/min is used; in testing fabrics the rate is greater than 15 percent/min and sometimes exceeds 100 percent/min. In order to minimize the outlay for testing equipment, a motor-driven screw jack was used to extend the fabrics. Also, it was desirable to keep the strain rate as low as possible and, it was hoped, close to that used with soil-testing equipment.

Size of Sample

To avoid end-restraint problems from necking down of the fabric, a 2:1 ratio of length to width was chosen for tensile-test samples. By using the 2:1 ratio and the maximum-allowable travel of the test equipment, a sample size 14.0 in long by 7.0 in wide was chosen. This size is larger than that of most ASTM fabric test samples and should account for the variability in the production of the fabric better than a smaller sample size would. In order to have 14.0 in of unsupported sample between the clamps, the samples were cut 27.0 in long by 7.0 in wide. The extra length was needed for overlapping the fabric in the end clamps.

Clamps

Three flat plates were bolted securely together to make a clamp for each end of the fabric samples. The plates were 16.0 in long by 3.0 in wide by 0.25 in thick. The samples were lapped between the three plates to prevent slippage during testing.

Number of Samples

With the numerous tests to be performed and 15 fabrics to be evaluated, it was decided that no more than three samples of each fabric could be tested if the project was to be completed within a reasonable time. Also, it was felt that three samples would be sufficient for determining an average strength value.

Warp Versus Fill

Samples 27.0 in by 7.0 in were cut from both the warp (perpendicular to the axis of the roll of fabric) and the fill (parallel to the axis of the roll of fabric) directions. Tensile tests were performed on these samples to determine whether the strength or elongation varied with the direction of the fabric, since little is known about this subject.

Tears

When silt fences are installed in the field, tears 0.5 in long are made in the fabric to fasten it to the supports by using wire or hog rings. It was decided that any reduction in strength that resulted from these tears should be determined. Therefore, three samples of each fabric cut in the warp direction and with single 0.5-in slits torn parallel to the length and in the middle were tested to determine the effects of the tears.

Table 3 gives the results of three tensile tests performed on each fabric in the warp direction, in the fill direction, and in the warp direction with a 0.5-in tear placed in the center of the samples. Load versus elongation curves were plotted for all samples. The strength values shown in Table 3 were developed as follows. If the fabric generated a load-elongation curve as indicated in Figure 2, curve A, the maximum load (P_{max}) was determined at the peak as shown. If the fabric generated a load-elongation curve as shown in Figure 2, curve B, P_{max} was determined at 20 percent elongation for the reasons noted earlier. If the load-elongation curve generated was similar to curve A but peaked past 20 percent elongation, then P_{max} was still taken as the load at 20 percent elongation.

The maximum strengths for the three samples of each fabric were averaged and divided by 7.0 in, the

Table 3. Average strength from tensile tests.

Material	Strength (lb/linear in)		
	Warp Direction	Fill Direction	Tear 0.5 in Long
Bidim C-22 (NW)	23	108	23
Mirafi 140 (NW)	53	43	50
Monofelt (NW)	20	30	28
Polyfelt TS-200 (NW)	22	2	31
Polyfelt TS-300 (NW)	26	3	27
Polyfelt TS-400 (NW)	27	5	25
Supac 4-P (NW)	4	21	4
Supac 5-E (NW)	3	7	7
Typar 3401 (NW)	49	62	45
Filter-X (W)	36	19	40
Laurel Erosion Cloth type I (W)	230	145	180
Laurel Erosion Cloth type II (W)	172	172	140
Monofilter (W)	134	135	158
Polyfilter GB (W)	91	95	74
Polyfilter X (W)	135	108	139

Figure 2. Determining maximum load (P_{max}) from tensile-strength data.

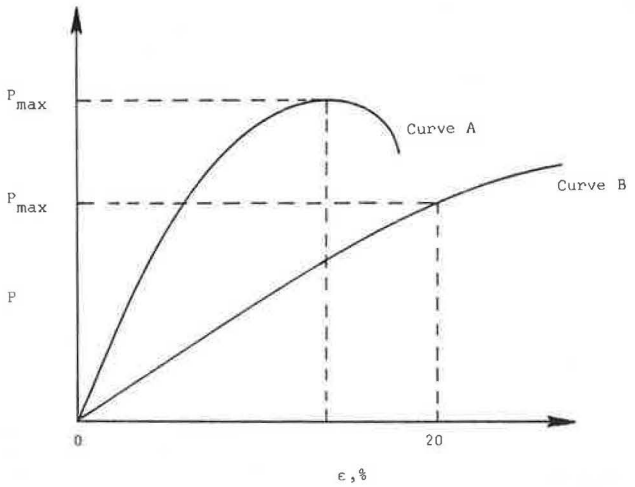

Table 4. Average strength from ultraviolet tests.

Material	Strength (lb/linear in)						
	Initial	1 Month	2 Months	3 Months	4 Months	5 Months	6 Months
Bidim C-22 (NW)	23	14	17	18	16	18	12
Mirafi 140 (NW)	53	11	11	5	-	-	-
Monofelt (NW)	20	9	8	4	-	-	-
Polyfelt TS-200 (NW)	22	17	17	15	14	14	2
Polyfelt TS-300 (NW)	26	17	20	18	13	17	14
Polyfelt TS-400 (NW)	27	20	18	28	31	18	24
Supac 4-P (NW)	4	6	5	4	-	-	-
Supac 5-E (NW)	3	6	5	8	6	8	11
Typar 3401 (NW)	49	28	24	22	23	19	18
Filter-X (W)	36	69	78	88	88	83	16
Laurel Erosion Cloth type I (W)	230	244	259	260	213	171	154
Laurel Erosion Cloth type II (W)	172	182	179	195	166	172	183
Monofilter (W)	134	211	220	227	193	194	200
Polyfilter GB (W)	91	124	78	136	155	163	122
Polyfilter X (W)	135	230	123	249	233	218	132

Note: Where no value is given, the fabric completely deteriorated and no samples were tested.

Table 5. Summary of weather data for ultraviolet tests.

Date	Rainfall (in)	Deviation from Normal Rainfall (in)	Average Temperature (°F)	Deviation from Normal Temperature (°F)	High Temperature (°F)	Low Temperature (°F)	Degree-Days
April 1977	2.15	-1.13	59.2	2.2	88	9	232
May 1977	2.70	-1.20	68.1	2.1	92	37	49
June 1977	1.56	-1.88	70.4	-2.9	91	45	18
July 1977	1.14	-4.02	80.0	2.9	103	53	0
Aug. 1977	2.37	-2.46	76.6	1.0	97	53	0
Sept. 1977	1.42	-2.77	71.9	2.5	96	50	4

Note: Degree-days are sums of negative degrees of average daily temperature from 65° as established by National Oceanic and Atmospheric Administration, U.S. Department of Commerce.

sample width. Table 3 gives the average maximum strengths.

The nonwoven fabrics, because of their construction and composition, indicate a lower strength value than the woven fabrics did, except for Filter X. The fill-direction strength is equal to or exceeds the warp-direction strength for 7 of the 15 fabrics tested. This trend is shown almost equally by the woven and nonwoven fabrics (three out of six woven fabrics and four out of nine nonwoven ones).

A comparison of the average strengths of the 0.5-in tear samples with those of the warp-direction samples shows that for nine of the 15 fabrics the former had average strengths equal to or exceeding those of the latter. This trend indicates that the stress on the fibers is realigned or transferred to unaffected fibers for small tears of 0.5 in. The remaining six fabrics (three woven and three nonwoven) indicate an average reduction in maximum strength of 20 percent (range 19-22 percent) for the woven fabrics and 7 percent (range 6-8 percent) for the nonwoven fabrics.

From a structural standpoint, it can be calculated that a silt fence 3.0 ft high and full of sediment needs to withstand an active earth pressure of 165 lb/linear ft of fence. This pressure amounts to a total load of 1650 lb against a fence 10 ft long or a warp tensile strength of approximately 50 lb/in. As indicated in Table 3, one nonwoven fabric (Mirafi 140) and all the woven fabrics except Filter X had a warp tensile strength, with or without the 0.5-in tear, in excess of this requirement. The

Table 6. Summary of recommendations.

Structure	Filtering Efficiency (%)	Flow Rate (gal/ft²/min)	Tensile Strength (lb/linear in)
3-ft silt fence with reinforced backing, posts 10 ft apart	75	0.3	Reinforcing governs
3-ft silt fence, no reinforced backing, posts 10 ft apart	75	0.3	50
18-in silt barrier, no reinforced backing, posts 10 ft apart	75	0.3	24
18-in silt barrier, no reinforced backing, posts 3 ft apart	75	0.3	7

remaining fabrics need support from something like woven wire to meet the requirement.

Because of the high cost of straw-bale barriers, consideration is being given to alternatives, particularly a small silt fence less than 18.0 in high (8), for use in drainage ditches and other locations. From a structural standpoint, the active earth pressure against this type of barrier would be 43 lb/linear ft of fence, for a total load of 430 lb against a section of fence 10.0 ft long. In order to withstand this load, the fence would need a warp tensile strength of 24 lb/in. From Table 3 it can be seen that all the fabrics except the nonwoven Bidim C-22, Monofelt, Polyfelt TS-200, Supac 4-P, and Supac 5-E meet the strength requirement for this type of filter barrier.

Since an 18.0-in filter barrier used in place of a straw-bale barrier would generally be a maximum of 10.0 ft long, it is desirable that the barrier posts not be spaced more than 3.0 ft apart. With this spacing, the needed warp tensile strength would be reduced to 7 lb/in. At this strength value, all but Supac 4-P and 5-E would meet the strength requirement without reinforcement.

Resistance to Damage by Ultraviolet Rays

To evaluate the susceptibility of the fabrics to damage from ultraviolet rays, a large sample of each fabric was hung from a clothesline, and each month three samples (27.0 in long by 7.0 in wide) were cut from it in the warp direction until the material decomposed or had undergone six months (April to October) of exposure. The samples were brought to the laboratory and tested for tensile strength.

Table 4 indicates the average warp tensile strength of the fabrics when exposed to the weather conditions indicated in Table 5. The months chosen for exposure are the ones of heaviest construction activity and the hardest on the fabrics. In addition, because most silt fences are helpful in the control of silt for three months and sometimes for as long as six months, the fabrics were evaluated over six months of exposure.

As indicated in Table 5, the rainfall for each month was from 1 to 4 in less than normal, whereas the air temperature was from 1 to 3°F above normal, except during June, when the average was 2.9°F less than normal.

After three months of exposure, three nonwoven fabrics (Mirafi 140, Monofelt, and Supac 4-P) deteriorated to the point that no samples could be obtained for testing. These three fabrics were the only untreated polypropylene or nonpolyester materials tested. Fabrics composed of polyester or black polypropylene material have good stability under exposure to ultraviolet rays. For all the woven and two of the nonwoven fabrics (Supac 4-P and 5-E) there was a gain in tensile strength after one month of exposure. The two nonwoven fabrics did not exhibit a large amount of tensile strength at any period of the testing. For Supac 5-E, however, there was an almost fourfold increase (from 3 to 11 lb/linear in) in strength after six months of exposure. Supac 4-P deteriorated after three months of exposure.

Of the nine nonwoven fabrics, three--Polyfelt TS-400, Supac 4-P, and Supac 5-E--showed essentially equal or greater tensile values after three months of weather exposure, whereas only two nonwoven fabrics, Polyfelt TS-400 and Supac 5-E, displayed this same trend after six months of exposure.

After three months of exposure, all the woven fabrics showed an increase in tensile strength over their original strength. Only Filter X and Laurel Erosion Cloth I indicated a substantial reduction in tensile strength after six months of exposure, whereas for the remaining four woven fabrics the strengths stayed essentially the same or increased.

CONCLUSIONS

In evaluations of fabrics for use in silt fences, the laboratory filtering-efficiency test should be performed by using a uniformly graded silty soil. The fabric should remove 75 percent of all the soil particles carried in the agitated, sediment-laden water and should allow the water to pass through at a rate of 0.3 gal/ft²/min or faster. Although 0.3 gal/ft²/min was chosen as the lowest flow rate desired, the rate needs to be increased without causing the filtering efficiency to drop below 75 percent.

The silt-fence analysis indicates that the reinforcing wire used behind a silt fence 3.0 ft high could be eliminated if the strength of the fabric exceeds 50 lb/linear in. For small silt barriers used to replace straw-bale barriers (less than 18.0 in high), the tensile strength should exceed 24 lb/linear in of width of the fabric if the support posts are 10.0 ft apart. If the posts are placed at 3.0-ft spacings, the tensile strength can be as low as 7 lb/linear in of width, and the barriers will be structurally sound without any reinforcement.

Table 6 summarizes these conclusions, which have been recommended to the Virginia Department of Highways and Transportation for purchasing specifications of silt fence filter fabrics.

IMPLEMENTATION OF FINDINGS

On the basis of the results of this study, the Virginia Department of Highways and Transportation has required all filter fabrics used for silt fences to meet or exceed the values shown in Table 6 on all construction projects advertised after April 1980. In conjunction with these specifications, the department is evaluating filter fabrics by the laboratory tests for filtering efficiency and warp tensile strength. These two tests were made effective October 1979. In the laboratory filtering-efficiency test a uniformly graded, silty soil is used to generate the sediment-laden mixture.

ACKNOWLEDGMENT

I would like to express my appreciation to M.O Harris, technician supervisor; G.T. Gilbert, former technician with the Virginia Highway and Transportation Research Council; and the several student helpers who spent many hours collecting data for the study. M.C. Anday, senior research scientist, and W.C. Sherwood, faculty research scientist, are

acknowledged for their valuable guidance and advice. Special thanks go to Barbara Turner for clerical assistance throughout the study and for typing this paper.

The opinions, findings, and conclusions expressed in this paper are mine and not necessarily those of the sponsoring agencies.

REFERENCES

1. 1979 Annual Book of ASTM Standards--Textiles, Part 32. American Society for Testing and Materials, Philadelphia, PA, 1979.
2. D.C. Wyant. Working Plan--Evaluation of Filter Fabrics for Use as Silt Fences. Virginia Highway and Transportation Research Council, Charlottesville, VHTRC Rept. 77-WP16, March 1977.
3. D.C. Wyant. Final Report--Evaluation of Erosion and Siltation Control Fabrics. Virginia Highway and Transportation Research Council, Charlottesville, VHTRC Rept. 76-R54, April 1976.
4. D.K. Todd, ed. The Water Encyclopedia. Water Information Center, Port Washington, NY, 1970.
5. Standard Methods for the Examination of Water and Wastewater. American Public Health Association, American Water Works Association, Water Pollution Control Federation, 14th ed, Washington, DC, 1976.
6. D.C. Wyant, W.C. Sherwood, and H.N. Walker. Erosion Prevention During Highway Construction by the Use of Sprayed-On Chemicals. Virginia Highway and Transportation Research Council, Charlottesville, VHRC Rept. 72-R1, July 1972.
7. W.C. Sherwood and D.C. Wyant. Installation of Straw and Fabric Filter Barriers for Sediment Control. Virginia Highway and Transportation Research Council, Charlottesville, VHTRC Rept. 77-R18, Sept. 1976.
8. Manual on Erosion and Sediment Control. Virginia Department of Highways and Transportation, Richmond, April 1980.

Publication of this paper sponsored by Committee on Hydrology, Hydraulics, and Water Quality.

Flood Frequency Analysis for Regulated Rivers

STEVEN G. BUCHBERGER

A case study of the Colorado River at Glenwood Springs, Colorado, is presented to demonstrate several statistical tests for identifying watersheds in which conditions are changing with time. Results of the tests indicate that annual peak flows of the Colorado River are influenced significantly by reservoir regulation. Consequently, conventional methods of frequency analysis are not suitable for obtaining flood estimates from the data series. Time-series analysis is a versatile approach to flood-frequency determinations when conventional statistical methods are not appropriate. The basic strategy of time-series analysis is to treat each value of the regulated annual peak-flow series as a combination of two elements--a deterministic component and a stochastic component. The deterministic component is quantified and removed from the flood series. The residual stochastic components, found to be stationary and independent, are then fitted to a probability distribution from which annual floods are estimated. Results of the time-series analysis show that the 2 percent and 1 percent chance floods, both required for Interstate highway design, are substantially less than corresponding log-Pearson type III estimates. Because the time-series analysis is able to detect and to treat the impact of reservoir regulation on the peak-flow series, the resulting flood frequency estimates are more representative of the watershed.

Analysis of the magnitude and frequency of floods is an important prerequisite of many engineering projects and consequently a routine practice in many engineering offices. During the past 60 years, a variety of techniques have been developed for peak-flow analysis (1). In an effort to promote a consistent approach to these peak-flow studies, the U.S. Water Resources Council (2-4) recommended the log-Pearson type III (LP III) distribution for determinations of flood frequency.

Because the LP III procedure is simple and well documented, it has become a popular method of flood flow determination. Application of this methodology, however, must not preclude engineering judgment. There are a growing number of situations--such as watersheds in which peak flows are altered by reservoir regulation--for which conventional statistical methods are inappropriate. The Colorado River in west central Colorado is a classic example. Experience has shown that myopic application of the LP III method results in flood estimates that are not representative of the Colorado River watershed.

The Colorado Department of Highways is now involved in final design of the uncompleted portions of I-70, much of which will parallel and at times cross the Colorado River. For public safety and project economy, it is imperative that the final design be based on peak-flow estimates that accurately reflect the flood characteristics of the Colorado River. The purpose of this paper, therefore, is to (a) present several objective methods for identifying watersheds in which reservoir regulation significantly influences annual peak flows and (b) demonstrate an alternate approach that combines time-series analysis and engineering judgment in order to obtain flood frequency estimates of regulated rivers.

BACKGROUND INFORMATION

I-70 is the major route for east-bound and west-bound traffic in Colorado. One of the few segments of I-70 that remains uncompleted is that through Glenwood Canyon, a narrow meandering gorge of sheer cliffs shaped over millions of years by the erosive action of the Colorado River. Although it is renowned for its scenic splendor, the canyon also serves as a vital transportation corridor for west central Colorado. Glenwood Canyon now accommodates US-6, the Denver and Rio Grande Western Railroad, and the Shoshone Dam and Power Plant of the Public Service Company of Colorado.

In 1969 the Colorado Department of Highways received and accepted a hydrologic report (5) of the Colorado River at Glenwood Canyon. The report included several LP III analyses for various periods of the annual flood record observed at Glenwood

Table 1. Flood frequency estimates of Colorado River at Glenwood Springs.

Annual Exceedance Probability	Estimated Flood Discharge[a] (ft^3/s)		
	LP III (1900-1968)	LP III (1942-1968)	Recommended for Design
0.50	16 350	11 900	16 000
0.02	31 000	22 000	25 000
0.01	33 250	23 400	26 500

[a]From Huggins and Griek (5).

Table 2. Peak flows of Colorado River at Glenwood Springs.

Year	Discharge (ft^3/s)	Year	Discharge (ft^3/s)	Year	Discharge (ft^3/s)	Year	Discharge (ft^3/s)
1900	20 000	1920	24 300	1940	11 100	1960	9 730
1901	20 000	1921	29 000	1941	14 900	1961	7 680
1902	12 000	1922	16 100	1942	16 800	1962	14 600
1903	16 500	1923	20 400	1943	13 000	1963	5 470
1904	16 500	1924	24 500	1944	10 600	1964	7 580
1905	22 500	1925	11 200	1945	10 600	1965	11 900
1906	22 100	1926	23 000	1946	9 720	1966	4 840
1907	20 400	1927	18 400	1947	14 200	1967	9 200
1908	11 500	1928	27 400	1948	16 600	1968	8 100
1909	27 900	1929	21 400	1949	16 300	1969	7 120
1910	14 600	1930	15 500	1950	10 100	1970	13 220
1911	15 200	1931	9 710	1951	14 400	1971	9 970
1912	27 700	1932	17 300	1952	20 800	1972	7 300
1913	12 400	1933	20 600	1953	14 000	1973	12 220
1914	28 100	1934	8 140	1954	4 060	1974	9 620
1915	13 400	1935	21 300	1955	5 400	1975	8 270
1916	14 800	1936	16 900	1956	12 600	1976	4 240
1917	29 400	1937	11 400	1957	18 900	1977	2 340
1918	30 100	1938	20 900	1958	16 000	1978	11 180
1919	12 300	1939	13 100	1959	8 480	1979	11 860

Springs, a community near the western end of the canyon. Results of the study (Table 1) show that the flood estimates obtained from the short record (1942-1968) are 30 percent less than those from the entire record (1900-1968). The values recommended for design were a compromise between the flood estimates obtained from both periods.

A recent review (6) of the recommended values suggests that they are not representative of the watershed. For example, the annual peak flows of the Colorado River (Table 2) show that the 50 percent chance flood has not occurred for 22 consecutive years. Intuitively, it seems unlikely that this should happen; mathematically, it is simple to evaluate the probability that this would happen. Since annual peak flows are considered independent events, the probability P that a flood will not be exceeded for n consecutive years is

$$P = (1 - P_e)^n \quad (1)$$

in which P_e is the probability that the flood will be exceeded in any given year. For the case under consideration, $P_e = 0.50$ and $n = 22$. Hence,

$$P = (1 - 0.50)^{22} = 0.000\,000\,24 \quad (2)$$

or the probability of not exceeding the 50 percent chance flood for 22 consecutive years is about 1 in 4 million.

The remote possibility of this dry spell indicates that the recommended 50 percent chance flood is overestimated. Although this type of check can be extended to the 2 and 1 percent chance floods, the results would be inconclusive because the length of the annual peak-flow record is short in comparison with the expected frequency of occurrence of rare floods. Nevertheless, it is reasonable to suspect that a high bias also exists for the recommended 2 and 1 percent chance floods. Although inflated estimates may be condoned for providing an extra margin of safety, overconservativeness is not warranted, since economy of the I-70 project is linked inextricably to the magnitude of the design discharge.

A more compelling reason for an updated flood study, however, stems from consideration of the rationale used to obtain the recommended flood estimates. The 1969 report recognized that reservoir regulation affected the latter period of the peak-flow series. Nonetheless, the entire flood record was retained for its greater statistical base and subsequently used in the frequency analysis. As such, recommended flood estimates were derived from data collected during a time that no longer reflects prevailing conditions in the watershed. The shortcoming of this approach is obvious. Analysis of nonrepresentative flood data yields nonrepresentative flood estimates.

Many statistical tests are available to evaluate the suitability of an annual peak-flow series for conventional flood frequency determinations. Several of these tests are demonstrated following a brief discussion of the key data assumptions on which the frequency analysis is based.

DATA ASSUMPTIONS

In any statistical treatment of annual flood flows, the data must be stationary and reliable. Stationariness requires that the properties of the annual flood series remain time invariant; reliability implies that the flood record is free of substantial errors caused by measuring, transmitting, recording, and processing data. Further, the flood record must be independent and homogeneous. Independence means that peak flows from one year are not influenced by peak flows from previous years; homogeneity requires that all peak flows be from the same parent population or collection of all possible outcomes of annual floods.

A "well-behaved" flood series--one that is stationary, independent, reliable, and homogeneous--is suitable for flood frequency analysis by conventional statistical methods such as LP III. These prerequisites are reiterated in the Water Resource Council's guidelines (3,4), which caution, "Assessment of the adequacy and applicability of flood records is therefore a necessary first step in flood frequency analysis...."

TESTING ANNUAL FLOOD SERIES

Test for Stationariness

An effective test for stationariness involves detection of significant long-term trends in the data series (7). Although it may be possible to fit high-order polynomial functions to the data series, it is desirable to use simple relationships in order to keep the analysis tractable. Therefore, a linear trend is investigated here. For this case, least-squares regression is used to express the annual peak flows as a function of time:

$$q_i = a + bt_i \quad (3)$$

where

a = regression constant,
b = regression coefficient, and
q_i = peak discharge observed during year t_i.

For a series that is stationary, the slope of the regression line is not significantly different than zero. So to test for stationariness, the following hypotheses are postulated: $H_0 : b = 0$ versus $H_1 : b \neq 0$. The appropriate test statistic is given by the following equation:

$$T = r[(n-2)/(1-r^2)]^{1/2} \sim t(n-2) \quad (4)$$

where r is the correlation coefficient of the linear regression and n is the amount of data in the series. The test statistic is assumed to be a random variable that has the t-distribution with n - 2 degrees of freedom. Let $t_c[1(\alpha/2)]$ be the critical value of the test statistic at the α-level of significance. Then H_0 is accepted if

$$|T| < t_c[1-(\alpha/2)] \quad (5)$$

Otherwise, H_0 is rejected. By using the 80-year flood record given in Table 2, least-squares regression gives the following:

$$q_t = 22\,037 - (180.4)t_i \quad (6)$$

where t_i is the year minus 1900 and r is -0.63. The minus sign in Equation 6 indicates that the annual peak floods of the Colorado River are decreasing with time. From any statistics book, at the 1 percent level of significance with n - 2 = 78, t_c = 2.65. Equation 4 gives T = -7.16. Since $|T| > t_c$, H_0 is rejected. Consequently, the annual peak-flow series of the Colorado River at Glenwood Springs is considered nonstationary.

Test for Independence

Serial correlation is a measure of the degree of linear dependence among successive observations of a series that are separated by k time units. For a series of annual floods, the units of k are given in years. If an annual flood series is independent in time, its serial correlation coefficients, denoted by r(k) in which k ranges from 1 to n - 1, are not significantly different than zero. To verify linear independence of the annual peak-flow series it is necessary to perform a test of significance for each serial correlation coefficient. From a practical standpoint, however, it is usually sufficient to check only r(1). For this case, the following hypotheses are postulated: $H_0 : \rho(1) = 0$ versus $H_1 : \rho(1) \neq 0$, in which $\rho(1)$ is the population value of the first serial correlation coefficient. If we assume a circular, normal, stationary series of annual floods, r(1) is given by the following:

$$r(1) = [\Sigma(q_i q_{i+1}) - n\bar{q}^2]/[(n-1)s_q^2] \quad (7)$$

where $\bar{q}$ is the mean of the annual flood series and s_q^2 is the variance. Because a circular series is one that closes on itself (q_n followed by q_1), the summation is taken over all n-values of the flood record. Under these conditions, confidence limits for r(1) are given by the following equation:

$$CL[r(1)] = \left\{-1 \pm z_c[1-(\alpha/2)](n-2)^{1/2}\right\}/(n-1) \quad (8)$$

in which $z_c[1-(\alpha/2)]$ is the critical value of the standard normal deviate for a two-sided test at the α-level of significance. If r(1) falls inside the confidence limits, H_0 is accepted (8).

The data from Table 2 give r(1) = 0.349. At the 1 percent level of significance, z_c = 2.576 and Equation 8 yields CL[r(1)] = (-0.301, 0.275). Since r(1) falls outside these limits, it appears that the annual flood series of the Colorado River is not independent.

Recall that this test is based on a stationary series. The requirement for stationariness is necessary because long-term trends introduce significant positive correlation into a series (9). If nonstationariness is manifest as a linear trend (for example, in Equation 3), the positive correlation expected at r(1) is given by the following equation:

$$r(1)^* = (b^2/12s_q^2)(n^2 - 2n - 2) \quad (9)$$

By using b = -180.4 from Equation 6, the positive correlation expected from the linear trend is r(1)* = 0.388. Subtracting r(1)* from r(1) gives a value that is not significantly different than zero. Because the apparent significant serial correlation results from a negative linear trend and not from dependence among successive peak flows, the annual flood series of the Colorado River at Glenwood Springs should be considered independent.

Another test for linear independence of an annual peak-flow series is as follows. Define a "turning point" T whenever $q_{i-1} > q < q_{i+1}$ or $q_{i-1} < q > q_{i+1}$. For an independent series, confidence limits for t are given by the following:

$$CL[T] = \left\{2(n-2) \pm z_c[1-(\alpha/2)][(16n-29)/10]^{1/2}\right\}/3 \quad (10)$$

The hypothesis that the annual peak-flow series is independent in time is accepted if T falls inside the confidence limits (10). For the annual flood series of the Colorado River, T = 45 and n = 80 - 3 = 77 since on three occasions observed peak flows are identical for two successive years. At the 1 percent level of significance, Equation 10 gives CL[T] = (40.6, 59.4). Since T falls inside the confidence limits, the annual floods of the Colorado River are considered independent. This conclusion agrees with the result of the serial correlation test.

Test for Homogeneity

Statistical tests designed to ascertain whether or not data are from different populations invariably require that the data be divided into two subsamples. For example, one common application is to test for significant differences in the characteristics of snowmelt floods and rainfall floods when both are present in the peak-flow series. For the Colorado River, however, the investigation concerns flood data that are changing with time. Therefore, in the test for homogeneity, annual floods observed during the early period of record will be compared with those observed more recently.

One method, which requires only that the data be independent, is the Mann and Whitney U-test (11). From a flood series that is ranked in order of decreasing magnitude, the following two statistics are calculated:

$$U_1 = uv + (u/2)(u+1) - R_u \quad (11)$$

$$U_2 = uv - U_1 \quad (12)$$

where u and v are the subsample sizes (u + v = n) and R_u is the sum of the ranks assigned to the sample of size u. Let U be the smaller of U_1 and U_2. Then the test statistic T is defined as follows:

$$T = [U - (uv/2)]/[(uv/12)(u+v+1)]^{1/2} \sim N(0,1) \quad (13)$$

If tied observations are present, the following correction is made:

$$C = (1/12)(t^3 - t) \quad (14)$$

in which t is the number of observations tied at a given rank and C is computed only for those tied observations that appear in both subsamples. The test statistic T now becomes the following:

$$T = [U - (uv/2)] / \left\{[uv/(n^2 + n)]\,[(n^3 - n)/12 - \Sigma C]\right\}^{1/2} \sim N(0,1) \quad (15)$$

For subsamples, both containing more than 20 observations, T is assumed to have the standard normal distribution. The hypothesis that both subsamples are from the same population is accepted at the α-level of significance if the following condition is met:

$$|T| < z_c\,[1 - (\alpha/2)] \quad (16)$$

By using the data given in Table 2, subsample 1 is taken as the data from 1900 to 1929 (u = 30) and subsample 2 covers 1930 to 1979 (v = 50). These subsamples yield R_u = 682, U_1 = 1283, U_2 = 217, and ΣC = 1.0. Equation 15 gives T = -5.36. At the 1 percent level of significance z_c = 2.576. Since $|T| > z_c$, the hypothesis that both subsamples are from the same population is rejected. Noting that the test for stationariness has previously identified a significant linear trend, the result of the Mann and Whitney U-test is expected.

Table 3. Tests to assess annual peak-flow series (1900-1979) of Colorado River at Glenwood Springs.

Condition	Test	Result[a]	Reference
Stationary	Linear trend	No	(7)
Independent	Serial correlation	Yes	(7, 8, 9)
Independent	Turning point	Yes	(7, 10)
Homogeneous	Mann and Whitney	No	(11)
Reliable	Examination	Yes	(4)

[a] Yes: does meet criteria for conventional flood frequency analysis; no: does not meet criteria for conventional flood frequency analysis.

Note on Reliability

The statistical methods reviewed thus far have roots in hypothesis testing. Similar techniques, however, are not effective for evaluating the reliability of flood information. Although flood records always contain inaccuracies, statistical tests are generally unable to discriminate between data variability due to chance fluctuation and data variability resulting from random error.

Nevertheless, there are several ways to screen the flood series for suspected errors. One is to compare the data against concurrent records from nearby watersheds. This check may signal discrepancies that warrant further investigation. In most cases, data reliability is not a controlling factor during flood frequency analysis (4).

Summary of Data Tests

Statistical methods have been presented to test an annual flood series for three properties: sta-

Figure 1. Watershed of Colorado River above Glenwood Springs.

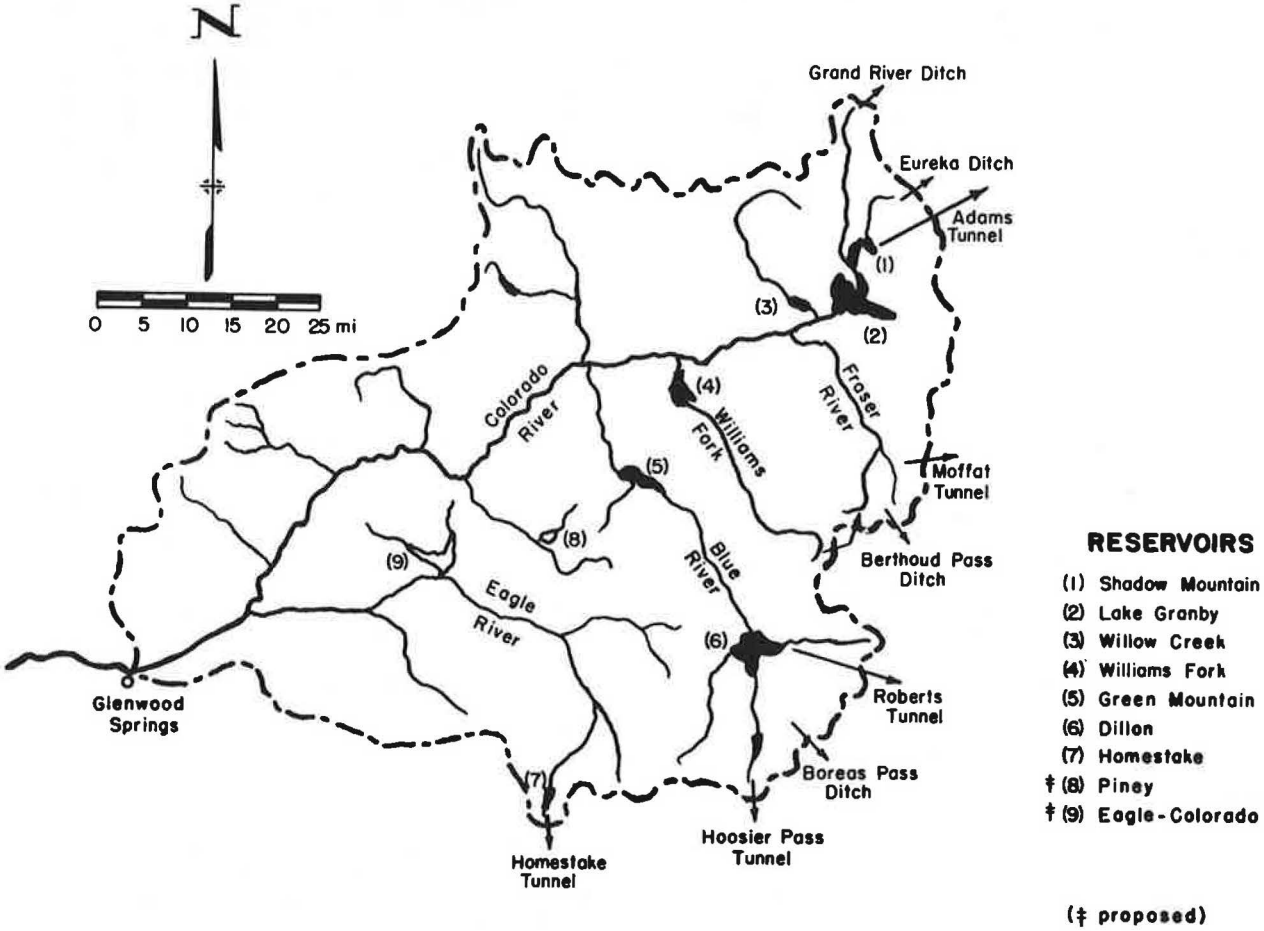

Table 4. Transmountain diversions from Colorado River and tributaries upstream of Glenwood Canyon.

Diversions	Year	Origin	Destination
Ewing Ditch	1880	Piney Creek	Arkansas River
Grand River Ditch	1892	Colorado River	Cache La Poudre River
Berthoud Pass Ditch	1909	Fraser River	West Fork Clear Creek
Boreas Pass Ditch	1914	Indiana Creek	Tarryall Creek
Fremont Pass Ditch[a]	1929	Tenmile Creek	Arkansas River
Columbine Ditch	1931	Eagle River	Arkansas River
Wurtz Ditch	1932	Piney River	Arkansas River
Moffat Tunnel	1936	Fraser River	South Boulder Creek
Eureka Ditch	1940	Colorado River	Big Thompson River
Gumlick Tunnel	1940	Williams Fork River	South Boulder Creek
Adams Tunnel	1947	Lake Granby	Big Thompson River
Hoosier Pass Tunnel	1952	Blue River	Middle fork of South Platte River
Roberts Tunnel	1963	Dillion Reservoir	North fork of South Platte River
Homestake Tunnel	1967	Eagle River	Arkansas and South Platte Rivers
Vidler Tunnel	1971	Montezuma Creek	Clear Creek

[a]Discontinued in 1943.

Table 5. Reservoirs from Colorado River or tributaries upstream of Glenwood Canyon.

Reservoir	Usable Storage (acre-ft)	Year Storage Began	Location	Operating Agency
Ralston	11 000	1937	East slope	DWB[a]
Marston	17 000	1939	East slope	DWB
Williams Fork	97 000	1939	West slope	DWB
Green Mountain	147 000	1942	West slope	WPRS[b]
Shadow Mountain	18 000	1947	West slope	WPRS
Lake Granby	466 000	1949	West slope	WPRS
Horsetooth	144 000	1951	East slope	WPRS
Willow Creek	10 000	1953	West slope	WPRS
Carter Lake	113 000	1954	East slope	WPRS
Gross	43 000[c]	1955	East slope	DWB
Montgomery	5 000	1957	East slope	CCS[d]
Dillion	254 000	1963	West slope	DWB
Homestake	43 000	1967	West slope	CCS
Strontia Springs	8 000	-[e]	East slope	DWB
Piney	40 000	-[f]	West slope	DWB
Eagle-Colorado	350 000	-[f]	West slope	DWB
Two Forks	860 000	-[f]	East slope	DWB, WPRS

[a]Denver Water Board. [b]Water and Power Resources Service. [c]To be increased to 113 000 acre-ft. [d]City of Colorado Springs. [e]Under construction. [f]Proposed.

Figure 2. Transmountain diversions from Colorado River watershed above Glenwood Springs.

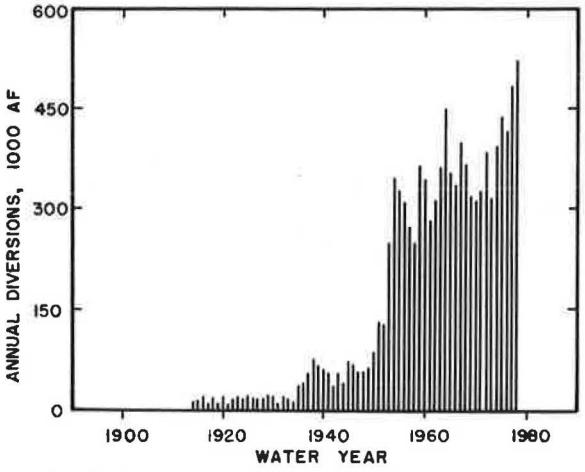

Figure 3. Annual peak flows of Colorado River at Glenwood Springs.

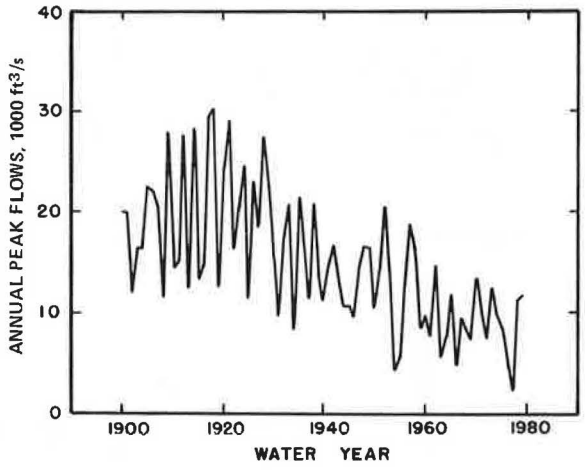

tionariness, independence, and homogeneity. Results of the tests applied to the annual peak-flow series of the Colorado River at Glenwood Springs are summarized in Table 3. The references cited in Table 3 demonstrate similar applications of other statistical tests available to aid practitioners involved in flood frequency analyses.

Results of the tests for stationariness and homogeneity reveal that conventional methods of analysis are not suitable for flood frequency determinations of the Colorado River at Glenwood Springs. Analysis of these data requires a technique that is sensitive to the sequential arrangement of the annual peak-flow series. This technique is known as time-series analysis. Before this methodology is presented, it is necessary to review the processes that affect the stream flow of the Colorado River above Glenwood Springs.

ANATOMY OF WATERSHED

Basin Description

From its headwaters high along the Continental Divide in Rocky Mountain National Park, the Colorado River flows southwest approximately 130 miles to Glenwood Canyon. Along this reach, as shown in Figure 1, five major tributaries--the Fraser, Williams Fork, Piney, Blue, and Eagle Rivers--join the Colorado River and contribute to a drainage area of 4560 miles^2.

Rugged snow-capped peaks, some rising more than 14 000 ft, frame the eastern boundary of the watershed. Below the headwaters, rolling alpine meadows yield to subalpine stands of aspen and conifer that make up extensive tracts of national forest. Drainage geomorphology evolves from intermittent streams of snowmelt cascading down glacial cirques to perennial meandering rivers flowing through broad U-shaped valleys. Although summer thunderstorms may cause appreciable flows on tributary reaches, annual peak flows on the Colorado River result from snowmelt runoff during the spring.

Diversions and Storage

The majority of Colorado's population live on the plains along the eastern foothills of the Rocky Mountains. In this arid region the water supply is not sufficient to support the demands of agricul-

Figure 4. Granby Reservoir, 1979 annual operating plan.

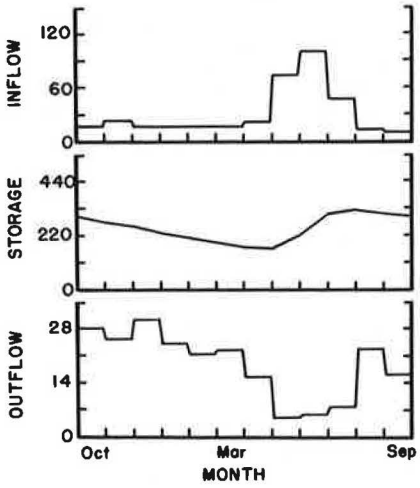

Figure 5. Annual peak flows of Colorado River at Granby.

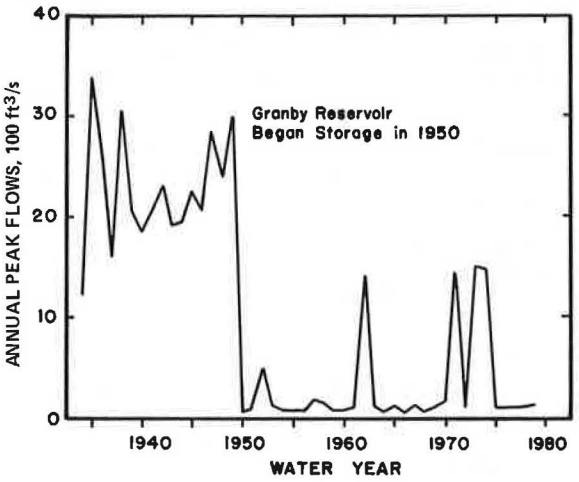

tural, industrial, and municipal interests. To supplement the stream flow of the eastern-slope rivers, snowmelt runoff from the Colorado River watershed is diverted through the Continental Divide to the eastern plains. The transmountain diversions that operate above Glenwood Canyon are given in Table 4.

The annual hydrograph of the Colorado River exhibits pronounced seasonality. During months of low stream flow, it is impossible to meet demands for transmountain water. To help ensure a reliable supply, a network of storage reservoirs has been constructed (Table 5). Note that the reservoirs located east of the Continental Divide receive water from the Colorado River via one or more of the diversions listed in Table 4.

The projects shown in Tables 4 and 5 demonstrate that development of water resources in the Colorado River watershed has proceeded at a rapid pace, especially during the past 50 years. This point is substantiated further in Figure 2, which shows the annual volume of water exported from the watershed since 1914. Plans for additional storage reservoirs testify that inevitable future development along the eastern foothills will increase demands for transmountain water, and hence the trend in Figure 2 is expected to continue.

Streamflow Records

The Colorado River at Glenwood Springs has been monitored since 1900 by the U.S. Geological Survey. A time-series plot of the annual peak flows of the river is shown in Figure 3.

Reservoir Operation

A distinct feature of Figure 3 is the downward trend of the annual floods, particularly evident since the 1930s. Recall that the test for stationariness has indicated that this negative trend is statistically significant--that is, the trend cannot be attributed only to chance variation. This trend is likely the result of man-made river controls. It would be difficult to isolate and quantify the impact of each transmountain diversion and storage reservoir on the annual peak-flow series. Although it is not the intention of this paper to provide such an account, a brief description of the runoff and water-exchange system is included.

The primary objective of the reservoir network is to smooth out the seasonal fluctuations that characterize the hydrograph of the Colorado River and its headwater tributaries. To exploit the time-transient availability of water, reservoir operation is synchronized closely with the annual cycle of snowmelt runoff. In practice this means that the usable storage of each reservoir typically reaches its lowest level of the year just prior to the time of peak runoff. The depleted storage levels, which result from reservoir releases to downstream users and to transmountain diversions during periods of low stream flow, are replenished during the peak snowmelt season. Thus, annual operation of the reservoir network is a repeated pattern of water storage and water release during periods of high flow and low flow, respectively. A typical example appears in Figure 4 (12).

It should be emphasized that the timing of the reservoir filling operation guarantees maximum impact of the annual peak flows of the Colorado River at Glenwood Canyon. Of course, reservoir releases to the Colorado River are necessary to honor downstream senior water rights or to satisfy minimum required stream flows. However, these releases occur during periods of low snowmelt and consequently do not affect the peak flow of the river.

Significant changes in the characteristics of the annual peak-flow series are inevitable consequences of stream flow regulation. For example, consider the regulatory effect of Granby Reservoir, which has been in operation since 1950. As shown in Figure 5, this date coincides with an abrupt change in the sequence of annual peak flows at this site. The impact of Granby Reservoir is demonstrated further with the data given below:

Statistic	Before Regulation	During Regulation
Year	1934-1949	1950-1979
Mean (ft^3/s)	2200	300
SD (ft^3/s)	550	470

In summary, the construction of numerous storage reservoirs and transmountain diversions has significantly altered the virgin conditions of the Colorado River watershed above Glenwood Canyon. These water projects appreciably affect the annual peak discharge of the Colorado River. Therefore, a flood frequency analysis of the annual flood series must consider the impact of historical development within the watershed.

Figure 6. CMA of annual peak flows of Colorado River at Glenwood Springs.

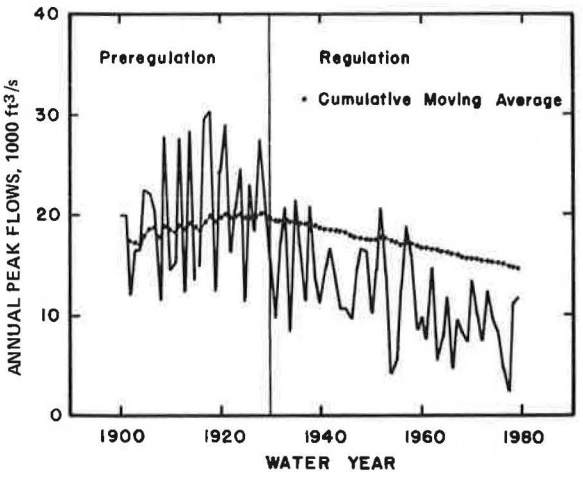

Figure 7. Linear-trend fit to regulation-period annual peak-flow series of Colorado River at Glenwood Springs.

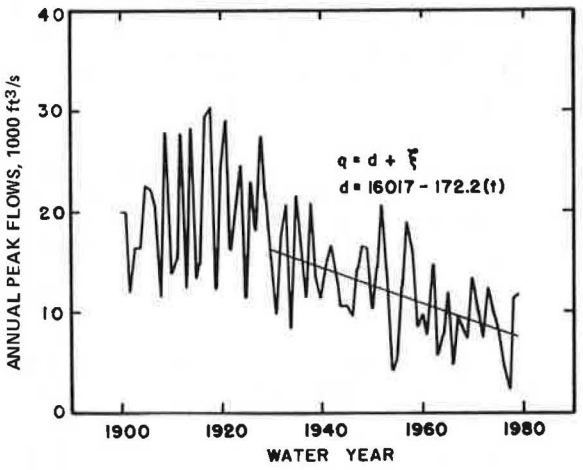

OPTIONS FOR ANALYSIS OF REGULATED ANNUAL PEAK FLOWS

Reservoir-Simulation Approach

One method used to estimate frequencies of regulated peak flows is to route the entire historical runoff record through the reservoir system and then analyze the outflows by graphical techniques (13). This method requires a watershed model capable of simulating the annual operation of all existing and proposed reservoirs. At present, no watershed model has been developed for the Colorado River upstream of Glenwood Canyon. Consequently, this approach is not a practical option for estimating flood frequencies of the Colorado River.

Time-Series Approach

Another method that does not require reservoir modeling but instead deals directly with the observed sequence of annual peak flows is time-series analysis. In the time-series approach, each value of the flood series is considered to be a combination of a deterministic component and a random, or stochastic, component. The deterministic component represents the linear trend in the series. This trend has been shown to reflect two peculiar properties of the data--nonstationariness and serial correlation. The basic strategy of time-series analysis, then, is to remove the deterministic trend and investigate the properties of the residual stochastic components. If the stochastic residuals satisfy the data assumptions needed for flood frequency analysis, they can be used to obtain flood frequency estimates of the Colorado River.

TIME-SERIES ANALYSIS

Preregulation and Regulation Periods

In Figure 6, superimposed on the annual peak flows of the Colorado River at Glenwood Springs is a sequence of solid circles that represents the cumulative moving average (CMA) of the series. The CMA for any given year is equal to the average value of all annual floods that have occurred from 1900 through that particular year. The CMA sequence reveals that since 1930 there has been a progressive decrease in the mean value of the annual peak-flow series. For the purposes of this time-series analysis, the annual peak-flow record is separated into two periods--preregulation and regulation. Considering the scenario of development within the watershed and noting the trend of the CMA, the preregulation period is designated by the years 1900-1929 and the regulation period by the years 1930-1979.

A shortcoming of many flood frequency studies is a lack of data. In this case, however, the central issue concerns the representativeness of the data. As documented earlier (Figure 5), reservoir regulation can appreciably alter the characteristics of the annual flood series. Therefore, in order to better reflect conditions of the watershed that today influence the stream flow of the Colorado River at Glenwood Canyon, the time-series analysis treats only the regulation series.

Quantifying the Trend

Each peak-flow value of the regulation series is assumed to be composed of two parts--a deterministic component and a stochastic residual, which is stated mathematically as follows:

$$q = d + \xi \tag{17}$$

where

q = annual peak flow,
d = deterministic component, and
ξ = stochastic residual.

The stochastic residuals constitute the portion of the regulation series attributed to chance variation. These residuals are assumed to be stationary, independent, and homogeneous random variables. The deterministic components represent the portion of the series described by any long-term trend. By definition, the outcome of a deterministic process is known for any appropriate input. Hence, the magnitude of the deterministic component is specified whenever its chronological position in the time series is given.

Following the same reasoning offered in the test for stationariness, the trend is assumed to be a linear decrease in the mean value of the regulation peak-flow series. By using least-squares regression, the deterministic linear trend of the regulation series is as follows:

$$d_i = 16\,017 - (172.2)t_i \tag{18}$$

where t_i is the year minus 1930 and r is 0.54.

Figure 8. Adjusted regulation-period annual peak flows of Colorado River at Glenwood Springs.

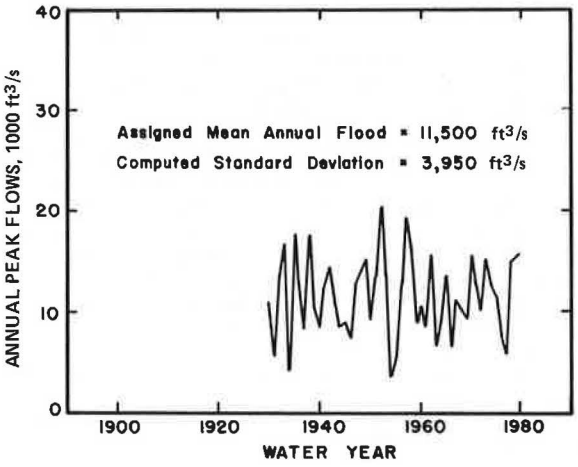

Table 6. Statistics for regulation-period annual peak flows (1930-1979) of Colorado River at Glenwood Springs.

Sample Statistic	Peak Flow[a]	Stochastic Residual[b]	Adjusted Peak Flow[b]
Mean (ft^3/s)	11 800	0.00	11 500[c]
SD (ft^3/s)	4 690	3950	3 950
Skewness	0.21	0.06	0.06

[a] Linear trend present. [b] Linear trend removed. [c] Assigned value.

This trend is shown as the straight line that extends from the year 1930 through 1979 in Figure 7. The test statistic given in Equation 4 indicates that the slope of this line is different than zero (α = 1 percent) and hence confirms the importance of the negative trend in the regulation-period annual flood series.

Removing the Trend

The stochastic residual is deduced as the difference between the observed peak flow and the deterministic component for each year of record or as follows:

$$\xi_i = q_i - d_i \tag{19}$$

Substituting Equation 18 into Equation 19 gives this equation:

$$\xi_i = q_i + (172.2)t_i - 16\,017 \tag{20}$$

The series of stochastic residuals has the following characteristics:

$$\bar{\xi} = 0 \tag{21}$$

$$s_\xi = (1 - r^2)^{1/2}(s_\phi) \tag{22}$$

where

$\bar{\xi}$ = mean of stochastic residuals,
s_ξ = SD of stochastic residuals, and
s_ϕ = SD of regulation-period annual floods.

In Equation 22, r^2 is the coefficient of determination of the linear regression and represents the percentage of s_ϕ^2 that is explained by the linear deterministic trend. The remaining, or unexplained, variance of the annual floods in the regulation series is attributed to the variance of the stochastic residuals.

SD of the regulation-period annual floods is as follows:

$$s_\phi = 4690\ ft^3/s \tag{23}$$

SD of the stochastic residuals is found by substituting Equation 23 and the correlation coefficient of Equation 18 into Equation 22:

$$s_\xi = 3950\ ft^3/s \tag{24}$$

Comparison of Equations 23 and 24 shows that removal of the deterministic component causes a substantial reduction in the SD-value. This result is expected since a measurable portion of the total variance of the regulation series is contributed by the deterministic trend.

The mean value of the regulation-period annual floods is as follows:

$$\bar{q}_\phi = 11\,800\ ft^3/s \tag{25}$$

However, Equation 21 shows that the residual series is centered about zero. Accordingly, some values of the residual series are negative. This is apparent by noting that about half the regulation-period peak flows are located below the linear trend in Figure 7.

Because some of the stochastic residuals are negative, they should not be interpreted as annual peak flows or be used in a flood frequency study. To remedy this condition, a representative mean annual peak flow must be selected and added to each value of the stochastic residual series. There are no equations to help redefine the representative mean annual peak flow. Instead, the decision is subjective. Specification of the mean annual flood must be tempered with an understanding of the conditions that prevail during times of peak runoff. At the high extreme, the value of 11 800 ft^3/s given in Equation 25 could be used and thereby preserve the mean peak flow of the regulation series. At the low extreme, extrapolation of the least-squares regression (Equation 18) shows that the mean peak discharge could approach zero cubic feet per second by 2020. The compromise is somewhere between these limits. Although future development within the watershed is planned (Table 5), it is unlikely that the future pace will continue at the past rate. Hence, extrapolation of the regression line probably does not offer a reliable indication of the future mean peak flow. Besides, other factors too complicated to be described by linear regression (e.g., downstream water rights and minimum required reservoir releases) will prevent the mean peak flow from approaching zero cubic feet per second. It seems more realistic, therefore, to select a value closer to the upper limit of 11 800 ft^3/s. Now, if we consider that the I-70 project through Glenwood Canyon is scheduled for completion in the mid-1980s and note that additional upstream reservoirs are not planned for completion until the 1990s, a value of 11 500 ft^3/s was selected as a conservative representative mean annual flood of the Colorado River at Glenwood Springs.

The adjusted regulation annual peak-flow series, obtained by adding the selected mean value of 11 500 ft^3/s to each stochastic residual, is shown in Figure 8. The statistics of the regulation peak-flow series, the stochastic residuals, and the adjusted regulation peak-flow series are summarized in Table 6.

Figure 9. Normal distribution fitted to histogram of adjusted regulation-period annual peak flow of Colorado River at Glenwood Springs.

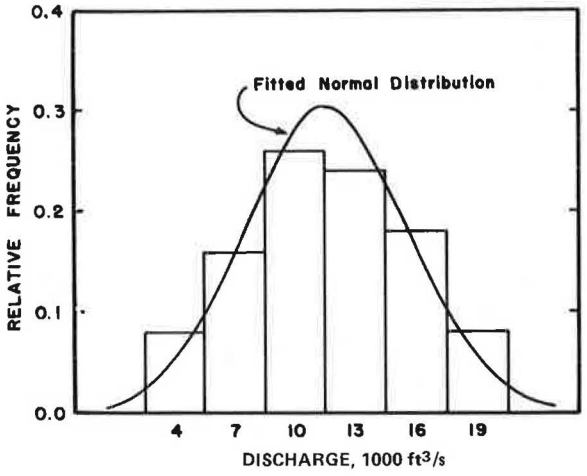

Table 7. Comparison of recommended flood-frequency estimates of Colorado River at Glenwood Springs.

Annual Exceedance Probability	Estimated Flow Discharge (ft^3/s)	
	1969 Study[a]	1979 Study[b]
0.50	16 000	11 500
0.02	25 000	20 000
0.01	26 500	21 000

[a]LP-III analysis of periods 1900-1968 and 1942-1968 (5).
[b]Time-series analysis of 1930-1979 (6).

ESTIMATING FLOOD FREQUENCIES

Testing Adjusted Flood Series

The data tests outlined earlier were used to investigate the properties of the adjusted regulation-period annual peak-flow series. Results show that the adjusted flood series is stationary, independent, and homogeneous. The adjusted series therefore qualifies for frequency analysis by conventional statistical methods.

Selecting the Distribution

The general relationship for estimating flood flows is as follows:

$$q_p = \bar{q} + k_p s_q \quad (26)$$

where

q_p = flood that has p percent chance of being exceeded in any year,
k_p = frequency factor for p percent chance flood,
$\bar{q}$ = mean of annual floods, and
s_q = SD of annual floods.

The frequency factor is a function of the selected exceedance probability and the distribution of the annual floods. To obtain flood estimates of the Colorado River at Glenwood Springs, then, it is necessary to fit the adjusted regulation-period annual floods to a probability distribution.

The skewness coefficient, a statistic that measures the symmetry of a data sample, is sometimes helpful in selecting a distribution (14). Because the skewness coefficient of the adjusted regulation-period annual floods is close to zero (Table 6), any symmetrical distribution is a reasonable candidate for the underlying probability distribution. Two possibilities are the normal distribution and the two-parameter gamma distribution.

The adjusted regulation-period peak-flow series was fitted to each distribution by the maximum-likelihood method (15). By using the chi-square test to check for goodness of fit, both the normal and the two-parameter gamma distributions were accepted (α = 1 percent) as suitable approximations for the theoretical distribution of the adjusted regulation-period annual floods. The normal distribution was selected to represent the adjusted series because, according to the chi-square test, it provided a slightly better fit than the two-parameter gamma distribution did. In Figure 9 the histogram of the adjusted regulation-period floods is shown with the fitted normal curve.

If we substitute the statistics of the adjusted series, Equation 26 becomes the following:

$$q_p = 11\,500 + z_p(3950) \quad (27)$$

in which z_p is the standard normal deviate that corresponds to the exceedance probability p. Equation 27 was used to estimate the flood flows of the Colorado River needed for design of I-70 through Glenwood Canyon. The results rounded to the nearest thousand in units of cubic feet per second are given in Table 7 under the heading for the 1979 study.

Discussion of Results

There may be some reluctance to accept flood flows estimated from a sample of adjusted data. Note, however, that individual values of the adjusted regulation-period annual flood series are byproducts of the methodology used to obtain the statistics of the adjusted series. Therefore, any concern should focus on the selected mean annual flood and the computed SD rather than on specific values of the adjusted flood series.

SD of the adjusted flood series is a direct analytical consequence of removing the linear deterministic trend from the peak-flow series. Of course, other types of trends could be investigated. However, because a linear relationship adequately describes the trend in the peak-flow series, there is no reason to pursue other more complicated trends that require estimation of additional regression parameters.

Although the mean value of the adjusted flood series was determined subjectively, the selection was based on careful consideration of existing and anticipated conditions in the watershed. This situation emphasizes that judgment remains an essential element in any flood-frequency analysis. For the purpose of estimating future flood flows, the computed values of SD and the assigned value of the mean annual flood are more representative of the watershed than are the statistics from the original flood series.

The results presented in Table 7 show that peak-flow estimates obtained with the time-series analysis are substantially less than those obtained previously with LP III analyses. The time-series approach was able to recognize and to treat the impact of reservoir regulation on the annual peak-flow series of the Colorado River. Therefore, the results of the time-series analysis more closely reflect the present-day character of the Colorado River at Glenwood Canyon.

CONCLUSION

Conventional methods of flood frequency analysis often are not suitable for watersheds in which conditions are changing with time. For such cases, a versatile alternative is time-series analysis, which considers the magnitude, the frequency, and the sequential order of the flood data. The time-series approach is formulated to reflect the factors and circumstances that significantly influence peak flows. Consequently, resulting flood estimates are representative of prevailing watershed conditions.

REFERENCES

1. B.M. Reich. Magnitude and Frequency of Floods. CRC Critical Reviews in Environmental Control, Vol. 6, No. 4, 1976, pp. 297-348.
2. A Uniform Technique for Determining Flood Flow Frequencies. Water Resources Council, Bull. 15, 1967.
3. Guidelines for Determining Flood Flow Frequency. Water Resources Council, Bull. 17, 1976.
4. Guidelines for Determining Flood Flow Frequency, rev. ed. Water Resources Council, Bull. 17A, 1977.
5. A.F. Huggins and M.R. Griek. Hydrologic Report of Colorado River-Glenwood Canyon. Barton, Stoddard, Milhollin and Higgens, Inc., Denver, CO, 1969, 34 pp.
6. S.G. Buchberger. Hydrologic Analysis of the Colorado River at Glenwood Canyon, Colorado. Colorado Department of Highways, Denver, Open-File Rept., 1979, 57 pp.
7. V. Yevjevich. Stochastic Processes in Hydrology. Water Resources Publications, Fort Collins, CO, 1972a, 276 pp.
8. C.T. Haan. Statistical Methods in Hydrology. Iowa State Univ. Press, Ames, 1977, 378 pp.
9. V. Yevjevich and R.I. Jeng. Properties of Non-Homogeneous Hydrologic Series. Colorado State Univ., Fort Collins, Hydrology Paper 32, 1969, 33 pp.
10. N.C. Matalas. Time Series Analysis. Water Resources Research, Vol. 3, No. 3, 1967, pp. 817-828.
11. G.W. Kite. Frequency and Risk Analyses in Hydrology. Water Resources Publications, Fort Collins, CO, 1977, 224 pp.
12. U.S. Bureau of Reclamation. Annual Operating Plan of Western Division, 1978-1979. U.S. Department of the Interior, 1978, 41 pp.
13. L.R. Beard and A.J. Fredrich. Hydrologic Frequency Analysis. Hydrologic Engineering Methods for Water Resources Development, Vol. 3, 1975.
14. V. Yevjevich. Probability and Statistics in Hydrology. Water Resources Publications, Fort Collins, CO, 1972b, 302 pp.
15. R.D. Markovic. Probability Functions of Best Fit to Distributions of Annual Precipitation and Runoff. Colorado State Univ., Fort Collins, Hydrology Paper 8, 1965, 33 pp.

Publication of this paper sponsored by Committee on Hydrology, Hydraulics, and Water Quality.

Dynamics Approach for Monitoring Bridge Deterioration

H.J. SALANE, J.W. BALDWIN, JR., AND R.C. DUFFIELD

In conjunction with a fatigue test of a full-scale in situ three-span highway bridge, an investigation was undertaken to evaluate the use of changes in dynamic properties of the bridge as a possible means of detecting structural deterioration due to fatigue cracks in the girders. Cyclic-loading tests (transient and steady-state) were conducted to determine the changes in dynamic properties. The loading was imposed by a moving-mass, closed-loop electrohydraulic actuator system. Several different dynamic tests were employed in the investigation to determine the modal viscous damping ratios, stiffness, and mechanical impedance of the bridge at selected intervals during the fatigue loading. Acoustic emission sensors were also used to monitor the growth of fatigue cracks in the girders. The results show that changes in the bridge stiffness and vibration signatures in the form of mechanical-impedance plots are indicators of structural deterioration caused by fatigue. Stiffness coefficients were calculated from the experimental mode shapes on the basis of a multi-degree-of-freedom system that uses modified coupling. The average reduction in stiffness was approximately 20 percent. This reduction was attributed to the combined deterioration of the bridge deck and steel girders. Mechanical-impedance plots were made from frequency-sweep tests, which included five resonant modes. Early changes in the mechanical-impedance plots were related to the deterioration of the bridge deck. Subsequent changes in these plots correlated with the fatigue cracking in the steel girders. An evaluation of the acoustic emission data showed that the sensors were able to detect the rapid critical crack growth in one girder.

At this time there is a substantial amount of research under way on the techniques used for monitoring structural deterioration. The types of techniques may be broadly classified under the following categories--nondestructive-testing methods and vibration-response methods. Much of the recent development in vibration-analysis techniques for monitoring structural integrity (1-4) stems from the needs of the offshore industry.

In general, nondestructive-testing procedures can be time-consuming and costly. This becomes evident when the structures are large, such as multispan bridges and offshore platforms. Nonetheless, the nondestructive tests that involve ultrasonic examinations and visual inspection are two of the most effective means of locating deterioration in a structure. As a consequence of the cost and time involved to accomplish nondestructive tests, alternative methods that will reduce the frequency of these tests are desirable.

Typically, a vibration-response method employs accelerometers to measure the response of the structure from either environmental forces or applied excitation forces. The data are analyzed to establish prescribed dynamic system parameters. Any significant changes in subsequent evaluations of these parameters are interpreted as fatigue damage in structural members or foundation settlement. In this approach to monitoring, vibration-response data provide a surveillance of the structure on a broad basis.

Many of today's highway bridges have a multitude of welded connections and details. These weldments

contain microscopic flaws from which cracks may initiate and propagate under service loading. Visual and ultrasonic examinations have shown that welded steel-girder bridges are prone to fatigue cracking. When a three-span continuous composite-girder highway bridge in Butler County, Missouri, was scheduled for removal, an in situ fatigue test to destruction of the full-scale structure was proposed. The aim of the study was to document the fatigue behavior of the bridge and to relate this behavior to the design specifications for highway bridges of the American Association of State Highway Officials (AASHO).

Another objective of the study was to evaluate several vibration-response methods for monitoring structural deterioration. This paper describes the evaluation of the following vibration-response methods: (a) transient, frequency-response, and sweep tests for the properties of an equivalent 1-degree-of-freedom (df) model, (b) steady-state normal mode tests for the properties of a multi-df model, and (c) acoustic emission measurements of fatigue-crack growth. Previous publications (5,6) contain a description of the instrumentation and data evaluation. For completeness, some material from the earlier publications is included in this paper.

DESCRIPTION OF TESTS

Four sets of dynamic tests were conducted on the in situ bridge. The first set was performed prior to initiating the fatigue tests. After 95 000 and 215 000 fatigue cycles, the fatigue test was interrupted and the second and third sets of dynamic tests were conducted. The fourth set of tests was performed at 377 000 fatigue cycles after the south interior girder had fractured at midspan.

In addition to the dynamic tests, 14 sets of acoustic-emission measurements at 8 locations on the girders were recorded without interrupting the fatigue test.

TEST BRIDGE

The two-lane, three-span [22, 28, and 22 m (72, 93, and 72 ft)] continuous composite-girder bridge was designed in 1962 in accordance with 1961 AASHO specifications for one-lane H15-44 loading. Principal features of the bridge are shown in Figure 1. Four flange girders of ASTM A-36 steel 76 cm (30 in) wide cover-plated over the main piers supported a 15-cm (6-in) concrete slab designed for composite action in the positive-movement regions. The slab concrete had a 28-day compressive strength of 36.3 MPa (5.27 ksi). Shear connectors were C4x5.4 channels 159 mm (6.25 in) long fillet-welded to the top flanges of the girders except in the cover-plated regions over the piers. The abutments and piers were supported by precast concrete piles driven to a minimum capacity of 0.285 MN (32 tons) in sand.

VIBRATION GENERATOR

Excitation force for all dynamic tests was supplied by a closed-loop electrohydraulic actuator system. Steel plates that weighed 4973 N (1115 lb) were attached to the top of the piston rod of the actuator. The actuator was mounted in the vertical position at designated stations on the upper side of the bridge deck. Locations of the actuator for the dynamic tests were at stations (Figure 2) 17, 16, 5, and 4 for the first bending mode, first torsional mode, second bending mode, and the sweep tests, respectively. During all the tests the maximum acceleration of the bridge deck was less than 0.7 g. The basic closed-loop system provided stroke and sinusoidal frequency control of the motion of the actuator. The excitation force was prescribed by controlling the relative acceleration of the moving weight with respect to the base of the actuator in a secondary control loop.

INSTRUMENTATION

Piezoresistive accelerometers that had a rating of 25 g were used to establish the relative acceleration of the moving weight and thereby control the excitation force that was applied during the dynamic tests. Servo accelerometers based on the Q-flex design with a range ±15 g were used to measure the vertical accelerations of the bridge at prescribed locations, which had been designated as stations, on the underside of the bridge. These stations are shown in Figure 2. Signals from the accelerometers were filtered with low-pass electronic filters set at 10 Hz.

DATA ACQUISITION

The primary data-acquisition system for the dynamic tests was an analog-to-digital converter and a tape transport. During the tests, the data channels were automatically scanned, sampled, and digitized at a prescribed rate of 70 or 100 times per second. The tape-transport unit wrote 12-bit data words into a nine-track magnetic tape at a density of 800 bits/in. For a backup data acquisition system, a light-beam multichannel strip-chart recorder was used to obtain an analog record of the test data.

TEST PROCEDURES

In the bridge test, each set of dynamic tests was made up of the following vibration-response techniques: (a) transient test, (b) frequency-response test, (c) sweep test, and (d) steady-state normal mode test.

For the transient, frequency-response, and normal mode tests, each test was conducted at three prescribed resonant frequencies of the bridge. The frequencies were associated with the following experimentally determined vibrational modes: (a) first (lowest) bending, (b) first (lowest) torsional, and (c) second bending. These modes were designated B1J, T1J, and B2J, respectively, in which J refers to the test set numbers, i.e., J = 1,2,3,4.

Transient Test

In the transient tests the bridge was excited to a steady-state condition at the frequency that corresponded to the prescribed mode. Then the hydraulics to the actuator was turned off. This produced a transient decaying response motion in the bridge. Thirty seconds of acceleration-response data were recorded at stations 17, 16, and 5 for modes B1, T1, and B2, respectively. Data from these tests were used to establish the damping ratio ζ from the log decrement curves.

Frequency-Response Test

The frequency-response tests were conducted to establish the frequency-response curves for each of the three vibrational modes. Response data for these curves were recorded at 30 increments of frequency. By this procedure a frequency range of ±0.2 Hz about the resonant frequency was covered. The bridge was allowed to reach a steady-state response condition at each increment of frequency prior to recording the accelerations at stations 5, 17, and

Figure 1. Test bridge.

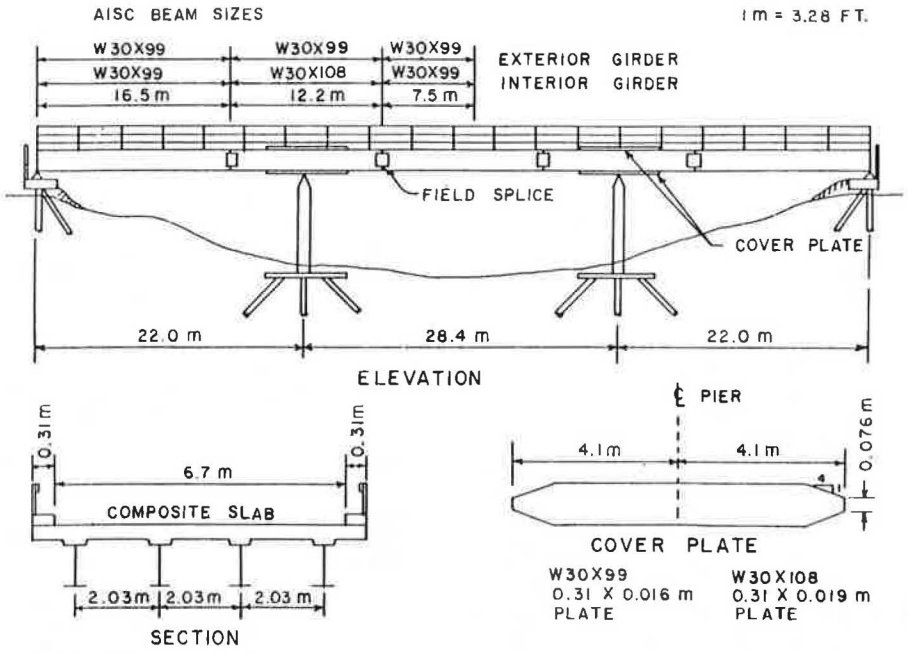

Figure 2. Accelerometer stations on bridge.

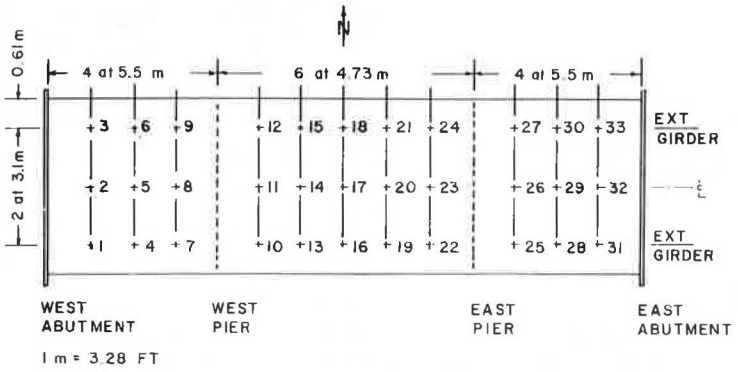

29 for the first bending mode; stations 4, 16, and 28 for the first torsional mode; and stations 5, 14, and 29 for the second bending mode. A constant excitation force was maintained during all tests. Response data were recorded for each frequency range beginning at the low end of the frequency range and increasing the frequency for each successive increment. Subsequently, the test was repeated beginning at the high end of the frequency range and decreasing the frequency for each successive increment. Data from these tests were used to calculate the damping ratio ζ by the half-power-bandwidth procedure.

Sweep Test

Sweep tests were performed to establish vibration signatures for the bridge in the form of mechanical impedance graphs. The frequency range of the sweep covered the lowest five experimentally determined resonant frequencies. A linear sweep rate of 0.02 Hz/s for a sine-wave excitation was used, and the test was initiated at the low end of the frequency spectrum. Continuous-response acceleration data were recorded at stations 4, 9, 15, and 30 during a 3-min time interval.

Normal Mode Test

Steady-state normal mode tests were conducted at each of the three resonant frequencies. One servo accelerometer was used as a fixed reference while the other accelerometer was moved from station to station to capture the response data. A minimum of 1024 data points was recorded at each station to establish the amplitude and phase of the steady-state motion with respect to the reference station. For the purpose of these tests the acceleration response was measured at 22 stations on the underside of the bridge. All 11 stations that were along the south exterior girder and all 11 stations along the north exterior girder were used. Stations along the centerline of the bridge were not used. From the test data, damping and stiffness coefficients of the bridge were calculated.

Acoustic-Emission Test

Eight acoustic-emission sensors were also used to monitor the growth of fatigue cracks in the steel girders during the fatigue test. State-of-the-art acoustic-emission equipment, which was readily available, was employed for this purpose. Each sensor was clamped to the bottom flange of a steel girder within 15 cm (6 in) of the end of a cover

plate. Sensors 1, 2, 3, and 4 were located in the west end span on the south exterior, south interior, north interior, and north exterior girders, respectively. Sensors 5, 6, 7, and 8 were located in the east end span on the south exterior, south interior, north interior, and north exterior girders, respectively. In operation, the sensors were individually monitored by manual switching. Fourteen sets of data were recorded during the course of the fatigue test. An amplitude count of acoustic emission per second over a 150-s interval was plotted versus time on an XY-recorder. In a time interval of 150 s, the bridge underwent approximately 300 cycles of vibration. The analog acoustic emission signals were amplified with gains that ranged from 72 to 82 dB. The resonant frequency of a sensor was 230 kHz, and an electronic filter was set to bandpass frequencies in the range of 100-400 kHz.

Acoustic-emission monitoring was initiated when the bridge had accumulated 56 000 fatigue cycles. At the outset of monitoring there appeared to be a repetitive noise in the emission signal when the center span of the bridge was in its most upward position. This noise was attributed to the vibration generator. Consequently, the acoustic-emission count was inhibited over that part of the vibration cycle. After 315 000 fatigue cycles, the inhibit circuitry was disconnected because of a malfunction in the electronics.

DISCUSSION OF RESULTS

The results from an evaluation of the data are presented to provide comparison of the various vibration-response methods. Lindner (5) and Brady (6) have provided a mathematical development of the equations used in the data evaluation.

Transient Test

On the basis that the bridge was excited in a single mode, the logarithmic-decrement method was applied to the decaying response data to determine the damping ratio ζ as a function of the number of free vibration cycles. Figure 3 illustrates the variation in ζ during a 35-cycle interval for test 2.

An alternate approach was adopted to evaluate the damping in tests 3 and 4 due to the multifrequency components that were observed in the transient-response data. Damping ratios were obtained by transforming the data from the time domain to the frequency domain. This procedure effectively separates the multifrequency components and is based on the properties of the discrete Fourier transform. Damping ratios for three modes in the four tests are listed in Table 1. The damping values for all three spans in each mode are consistent. It is also apparent that the damping increased from test 1 to test 2 and then decreased in tests 3 and 4.

Frequency-Response Tests

Analog data from the frequency-response tests were filtered by means of a 10-Hz low-pass filter prior to the analog-to-digital conversion. However, because of other frequency components in the response, the digital data were further filtered by a fast-Fourier-transform technique in order to isolate the amplitude of the response at each specific frequency increment. Figure 4 illustrates response graphs for the first bending mode, test 3. On the basis of the half-power bandwidth, the values of ζ that were calculated are listed in Table 2. Although there is a variation in the damping values between each span and for each set of tests, the range of ζ is consistently between 1 and 3 percent. The damping ratios reported in Table 2 are average values from the data obtained when the test was initiated at the low end of the frequency range and then subsequently repeated beginning at the high end of the frequency range.

Sweep Test

Mechanical impedance is defined as the ratio of the excitation force to steady-state velocity for sinusoidal motion. The resulting ratio is a complex quantity that may be represented by a magnitude and phase angle. If the force is applied at one location on the structure and the response velocity is determined at another location, the ratio is referred to as transfer impedance. However, if the force and velocity are located at the same place in the structure, the ratio is referred to as driving-point impedance. Minimum points on the mechanical impedance graph are associated with a resonant frequency of the structure. At resonance the phase angle between the excitation force and the response velocity is zero (or 180 degrees). Maximum ordinates on the impedance graph are called antiresonant points.

The intent in the sweep test was to maintain a constant force level throughout the frequency range. However, the amplitude controller was not able to maintain this condition at the high end of the frequency range. For a linear elastic system the mechanical impedance is independent of the excitation force. The frequency-response test data did not exhibit the jump phenomenon in the vicinity of the resonant response, which would have been an indication of nonlinear behavior. Thus, the assumption that the bridge was a linear elastic system was reasonably valid.

Figures 5 and 6 illustrate the variation in driving-point and transfer impedances for tests 3 and 4. A notable change in the impedance occurred between tests 1 and 2. The resonant frequencies decreased and the magnitudes of the impedance increased. This increase implies that the equivalent damping increased. The reduction in resonant frequencies was associated with the deterioration of the bridge deck.

The change in impedance between tests 2 and 3 was minimal. However, the lower resonant frequencies increased slightly, which was unexpected. The largest variation in impedance between tests 3 and 4 occurred at the higher resonant frequencies. Test 4 was conducted after the fracture had occurred in the south interior girder at the midpoint in the center span.

Normal Mode Test

Four sets of normal mode tests at three resonant frequencies were performed to evaluate the stiffness and damping properties of the bridge as the fatigue test progressed. A spectral analysis of the data revealed a harmonic component in the first-bending-mode data from tests 3 and 4. Figure 7 illustrates that the amplitude of the harmonic increased between tests 3 and 4. The harmonic in test 4 was anticipated because of the fracture in the girder. In the first bending mode the fracture was located at a point of maximum deflection, whereas in the second bending mode the fracture was located at a point of zero deflection (i.e., a vibrational node). However, in the torsional mode, the fracture was located at a point of one-half the maximum deflection, but the spectrum of the torsional data did not reveal any harmonics.

In order to establish the amplitudes for the mode shapes, all data were digitally filtered by an ex-

Figure 3. Damping ratio from logarithmic-decrement method.

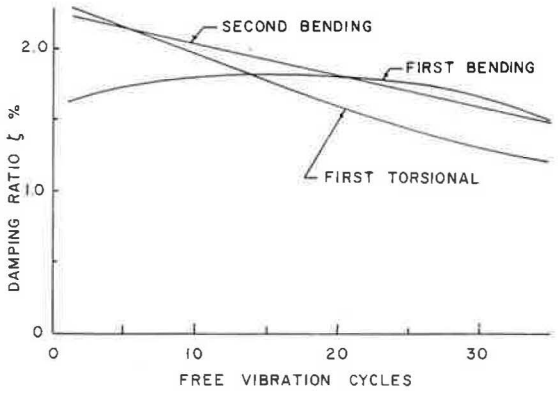

Table 1. Damping ratios and frequencies determined by Fourier-transform decay method.

Test No.	Frequency (Hz)	Damping Ratio (% critical) by Span		
		East	Center	West
First Bending				
1	2.92 (2.90)[a]	1.0	1.1	1.0
2	2.66 (2.73)	2.6	2.5	2.5
3	2.67	2.2	2.2	2.1
4	2.49	2.9	--	2.5
First Torsion				
1	3.62 (3.60)	1.7	1.6	1.7
2	3.34 (3.42)	3.3	3.3	--
3	3.11	3.2	3.1	3.0
4	3.19	2.6	2.7	2.7
Second Bending				
1	4.59 (4.57)	1.1	--	1.3
2	4.23 (4.28)	2.8	--	2.7
3	4.29	2.1	2.1	2.2
4	4.14	2.2	2.1	2.1

[a]Numbers in parentheses indicate damped natural frequency determined from the time-transient response signal.

tended cosine-bell window and analyzed by a fast-Fourier-transform technique. The spectral amplitudes were also normalized with respect to the spectral amplitudes at the reference station.

Since the bridge was assumed to have 22 df for vertical motion and three vibrational modes were measured, 66 equations were established to determine the stiffness and damping properties for the analytical model from the normal mode equations of motion. Because of the limited number of simultaneous equations, the coupling between the 22 nodes in the analytical model was arbitrarily assumed so that the bandwidth of the stiffness and damping matrices was 5. For the assumed coupling and utilizing symmetry, there are 63 unknown coefficients in the 22-df stiffness and damping matrices. The diagonal coefficients were assumed to be most significant and were used to monitor the change in properties during the fatigue test.

Figure 8 illustrates the relative changes in the stiffness coefficients between tests 1 and 3 and tests 1 and 4 for the stations on the north and south sides of the bridge. For the most part the reduction in stiffness coefficients was greater between tests 1 and 4 than between tests 1 and 3. The reduction in stiffness between tests 1 and 4 was also greater for the south side of the bridge, which correlates with the fracture in the south interior girder. The reason for the large variation in the coefficients for the east end of the bridge is not known.

Figure 4. Frequency response, test 3, first bending, center span.

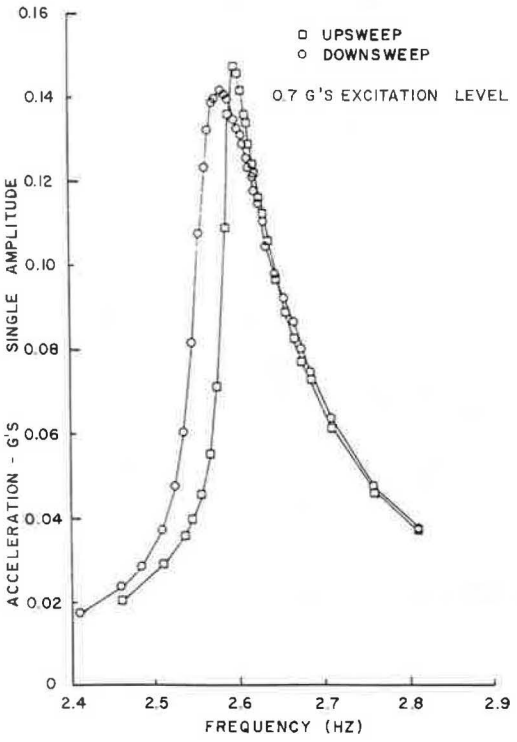

Table 2. Damping ratios determined from half-power-bandwidth method.

Test No.	Damping Ratio (% critical) by Span		
	East	Center	West
First Bending			
1	1.59	1.54	1.60
2	1.22	1.18	1.23
3	1.44	1.38	1.43
4	2.02	1.96	2.02
First Torsion			
1	2.00	1.82	1.98
2	2.06	1.82	1.95
3	1.40	1.39	1.36
4	2.30	1.88	2.17
Second Bending			
1	1.44	1.86	1.32
2	1.56	2.35	1.37
3	1.53	2.66	1.36
4	1.31	2.42	--

Acoustic-Emission Test

When a structure is under load, elastic stress waves called acoustic emissions are generated by plastic deformations that occur at imperfections in the material. These emissions can be detected by a

Figure 5. Driving-point impedance, tests 3 and 4, west span.

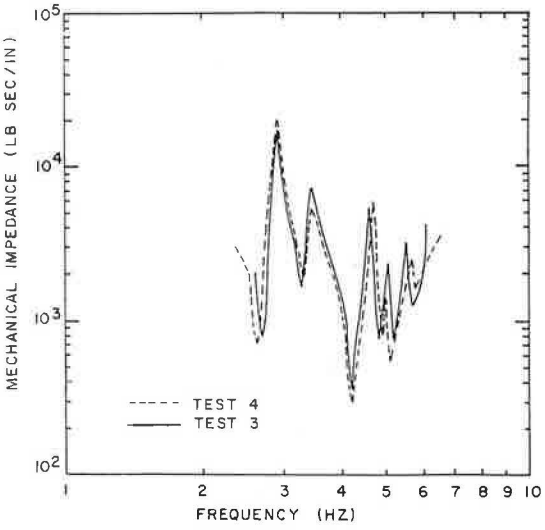

Figure 6. Transfer impedance, tests 3 and 4, center span.

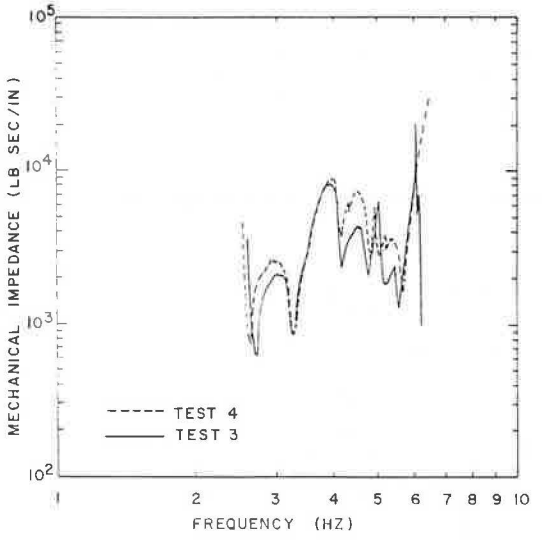

piezoelectric sensor. In the bridge tests, the analog signal from the sensors was converted to an amplitude count analogous to the amplitude of the oscillations in the sensor. Essentially, the sensor converted low-level stress waves to transient electrical signals that corresponded to resonant oscillations of the piezoelectrical element. The amplitude count was based on a time interval the duration of which was proportional to the peak amplitude of the oscillations of the piezoelectric sensor element.

The XY-graphs of amplitude versus time for intervals of 150 s on an intermittent basis did not display the data in a form convenient for evaluating probable crack growth in the welds and base metal where the cover plates terminated. Hence, the amplitude counts were digitized, and a mean value and a standard deviation were calculated for each 150-s interval.

Mean values of the amplitude count per second for each of the 14 data sets for sensors 2 and 6 are shown in Figure 9. These sensors were located on the south interior girder approximately 60 ft from

Figure 7. Spectra of first bending mode response, center span, tests 3 and 4.

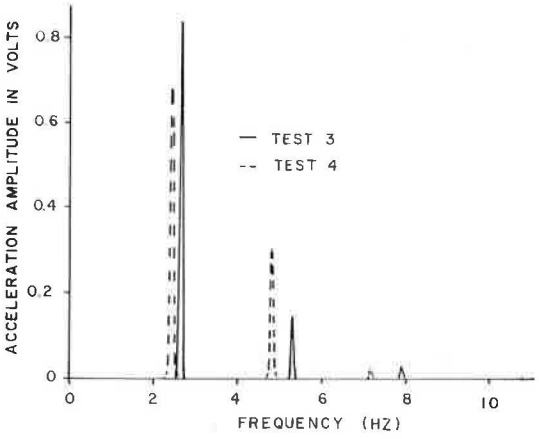

the location of the impending fracture at midspan. Figure 10 illustrates the amplitude count for sensors 1 and 8. Sensor 8 was located on the north exterior girder in the east span and sensor 1 was located on the south exterior girder in the west span. The amplitude count for all sensors was at its maximum at 370 000 fatigue cycles. This notable high count was attributed to the fracture that was probably occurring when the acoustic-emission data were recorded. Visual observation established that the fracture had completely severed the bottom flange and web of the girder approximately 25 min after these data were obtained.

Failures also occurred in the girder flanges within 3 ft of sensors 1 and 6. Ultrasonic inspections revealed these failures after 462 000 and 453 000 fatigue cycles, respectively. The maximum nominal tensile stress due to dead load, ballast, and inertial load at these locations was 103 MPa (15 ksi). However, the growth of fatigue cracks at these locations was not discernible in the recorded emission count.

SUMMARY AND CONCLUDING REMARKS

The intent of this study was to evaluate several vibration-response methods for monitoring structural deterioration. These methods were applied during a fatigue test to determine prescribed dynamic properties of a full-scale bridge.

The damping ratios range between 1 and 3 percent. There were indications that the damping increased and subsequently decreased. The increase may have been caused by mechanical abrasion between adjacent surfaces in the cracks in the concrete deck. Once the cracks became large, the abrasive action ceased and this form of energy dissipation was eliminated. The slipping of the guardrail connections and the friction in the girder support hinges and rocker bearings also contributed to the overall damping. During the fatigue test the variation in damping ratios was not significant from the viewpoint of structural monitoring.

Mechanical impedance is a direct approach to establish typical vibration signatures for a structure. However, there may be a drawback to using impedance as a vibration signature. Impedance (force/velocity) has the characteristics of damping, and damping is the least-known property of a structure.

Stiffness changes, in principle, are directly related to structural deterioration. Resonant frequencies are also a measure of deterioration because

Figure 8. Change in diagonal coefficients of stiffness matrix.

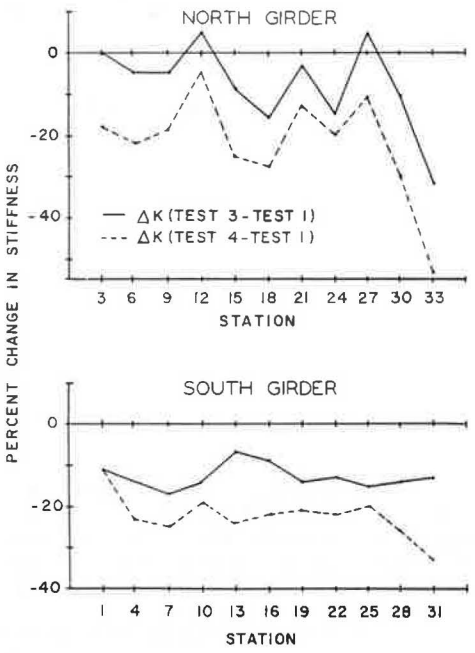

Figure 9. Acoustic emission amplitude count during fatigue test, sensors 2 and 6.

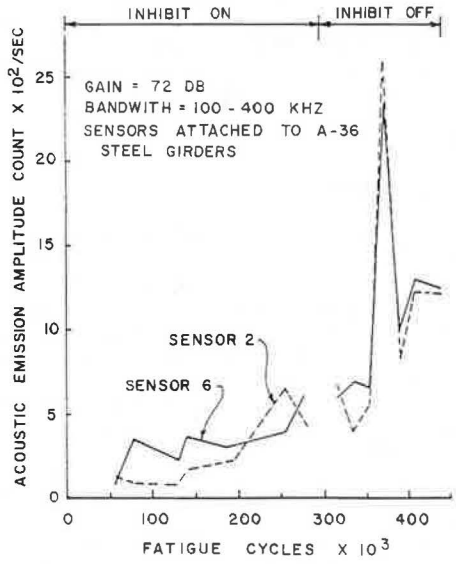

they are proportional to the square root of stiffness. On the basis of an arbitrary analytical model, a change of 20-40 percent in selected stiffness coefficients was observed. However, there was no apparent clue to the location of the fracture in the south interior girder from the changes in the stiffness coefficients for the 22-df model with its restricted coupling. To better simulate the physical behavior of the bridge by coupling all 22 df would require that 12 experimental modes be determined.

Changes in mode shapes were also indications of structural deterioration. When mode shapes are used for this purpose, the vibrational modes should be selected to provide significant response of the particular members that are being monitored. This

Figure 10. Acoustic emission amplitude count during fatigue test, sensors 1 and 8.

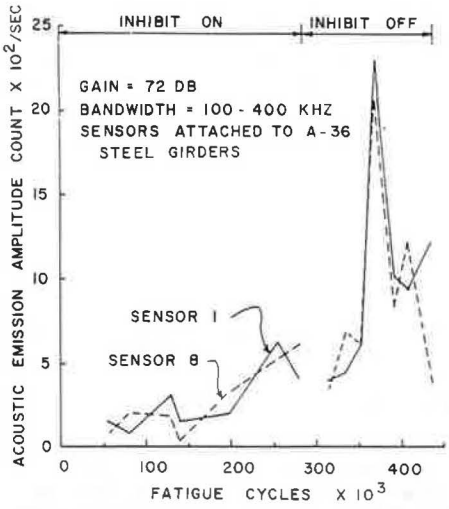

was evident when only the first-bending-mode shape in the bridge showed a marked change after the fracture in the girder.

The relatively slow growth of fatigue cracks in the critical fatigue regions under cyclic loading was not discernible with the acoustic-emission setup used in the bridge test. Extraneous noise from the hydraulic actuator and movement of the bridge on its supports tended to interfere with the acoustic-emission signals. Concrete undergoing permanent deformation also has emission signals that are higher than those from most metals.

All eight sensors were able to detect the critical crack growth in the south interior girder. The use of acoustic-emission sensors shows considerable promise for monitoring structural deterioration under dynamic service loads.

ACKNOWLEDGMENT

We are pleased to acknowledge with gratitude the following individuals and organizations for their contributions to this study: Missouri State Highway Department for sponsoring the project; U.S. Army Corps of Engineers for providing the test bridge; Federal Highway Administration for the use of a data acquisition system and providing the services of Harry Latz, engineering technician; and Robert K. Brady and Ivan E. Lindner, former graduate students, for evaluating the data and reporting the results in their M.S. theses.

REFERENCES

1. R.D. Begg and A.C. McKenzie. Monitoring of Offshore Structures Using Vibration Analysis. Proc., Illuminating Engineering Society Symposium on Integrity of Offshore Structures, Glasgow, Scotland, April 1978.
2. J.K. Vandiver. Detection of Structural Failure on Fixed Platforms by Measurement of Dynamic Response. Proc., Offshore Technology Conference, Vol. 2, OTC 2267, May 1975, pp. 243-252.
3. M.E. Wojnarowski, S.G. Stiansen, and N.E. Reddy. Structural Integrity Evaluation of a Fixed Platform Using Vibration Criteria. Proc., Offshore Technology Conference, Vol. 3, OTC 2909, May 1977, pp. 247-256.

4. R.N. Coppolino and S. Rubin. Detectability of Structural Failures in Offshore Platforms by Ambient Vibration Monitoring. Proc., Offshore Technology Conference, Vol. 4, OTC 3865, May 1980, pp. 101-110.
5. I.E. Lindner. Dynamic Behavior of a Composite Highway Bridge. Univ. of Missouri-Columbia, Columbia, M.S. thesis, 1976.
6. R.K. Brady. An Experimental Study of the Dynamic Characteristics of a Composite Highway Bridge. Univ. of Missouri-Columbia, Columbia, M.S. thesis, Aug. 1977.

Publication of this paper sponsored by Committee on Dynamics and Field Testing of Bridges.

Fatigue Cracks and Their Detection

J.W. BALDWIN, JR., H.J. SALANE, AND R.C. DUFFIELD

A three-span continuous composite bridge of modern design was field tested under fatigue loading that produced stresses equal to or greater than design stresses. During the fatigue loading, a regular inspection schedule was carried out by using radiographic, ultrasonic, and visual methods. Ultrasonic inspection was the most reliable and, in the regions inspected regularly, no cracks are known to have grown to a length greater than 38 mm (1.5 in) before detection. Radiography was nearly as reliable as ultrasonic inspection where it could be used, but more than half the material to be inspected was inaccessible to radiography. A total of 18 fatigue cracks developed at the ends of welded cover plates and 2 fatigue cracks developed in base metal not adjacent to welds. At 471 000 cycles of loading, these cracks had propagated far enough to completely sever the girder flanges at five different sections. The fatigue life in regions where the stress range was 155 MPa (22.5 ksi) was considerably longer than would be predicted on the basis of current code requirements. However, the fatigue life in regions where the stress range was only 60 MPa (8.7 ksi) was considerably shorter than would be predicted on the basis of current code requirements.

During the past two decades, concern about the potential for fatigue failures in highway bridges has increased dramatically. Major laboratory studies have been carried out to determine load versus fatigue-life relationships and to establish design criteria (1,2). The design code of the American Association of State Highway Officials (AASHO) (3), which made little reference to fatigue considerations in the 1950s, now contains highly restrictive fatigue considerations that virtually eliminate certain types of construction. An intensive inspection program has been instituted by the Federal Highway Administration (FHWA) to evaluate the condition of bridges that were designed and constructed before fatigue was recognized as a serious problem.

Laboratory studies are by far the most efficient and cost-effective means of determining fundamental behavior modes in structures, but a certain amount of extrapolation is always required when design criteria for full-scale structures are developed from laboratory data. This is particularly true in the case of fatigue because fatigue behavior is highly sensitive to fabrication details, which are extremely difficult to model in scaled-down laboratory studies. Thus, an occasional check of design criteria through testing of full-scale structures under controlled loading conditions is highly desirable. An unusual opportunity to conduct such a test was created when flood-control work by the U.S. Army Corps of Engineers on the St. Francis River in southeast Missouri necessitated the removal of a 12-year-old highway bridge.

OBJECTIVES

The entire bridge was to be loaded cyclically at stress levels equal to or greater than service-load stresses until one or more girders failed. Objectives of the test were twofold. First, the fatigue behavior of the bridge was to be observed and compared with both laboratory results and current design criteria.

Before loading began and periodically during the test, the bridge was to be inspected by using several modern crack-detection techniques. The second objective, then, was to compare these techniques and to evaluate the effectiveness of each. This was to be the equivalent of inspecting a bridge every few years for its entire lifetime under normal service conditions. Since small cracks missed during one or more inspections would eventually grow into large cracks or failures, this procedure would provide information concerning sizes and types of cracks that are likely to be missed as well as those that are likely to be found.

DESCRIPTION OF TEST BRIDGE

The two-lane bridge was made up of three [21.9, 28.3, and 21.9 m (72, 93, and 72 ft)] continuous concrete-on-steel composite-girder spans. It was designed during early 1962 according to 1961 AASHO specifications for one H15-44 loaded lane. [For a general schematic of the bridge, see Figure 1 in Salane, Baldwin, and Duffield in this Record; see also the report by Salane and others (4).] Girders and cover plates were of American Society for Testing and Materials (ASTM) A36 steel, and the unshored slab was cast from concrete with a 28-day compressive strength of 36.6 MPa (5720 psi). Shear connectors were C4x5.4 channels 159 mm (6.25 in) long fillet-welded to the top flanges of the girders.

Channel diaphragms 460 mm (18 in) deep bent from 610x8-mm (24x0.31-in) plates were bolted to 114x9.5-mm (4.5x0.38-in) bearing stiffeners over the supports and to 76x9.5-mm (3x0.38-in) web stiffeners in the spans. There were two intermediate diaphragms in each end span and four intermediate diaphragms in the center span.

DESCRIPTION OF FATIGUE TEST

A total of 471 000 fatigue cycles were applied to the bridge over a period of approximately five weeks. Desired dynamic stress ranges were obtained by exciting the bridge at its first-bending-mode resonant frequency by using the closed-loop electrohydraulic shaker shown in Figure 1. This shaker consisted of 40 kN (9 kips) of steel weights attached to the top of an 89-kN (20-kip) servocon-

trolled hydraulic actuator that was bolted to the girders through the deck slab at the center of the bridge. During fatigue loading, approximately 178 kN (40 kips) of concrete ballast was anchored to the deck slab at the center of each span. This ballast produced a mean stress on which the cyclic stress was superimposed so as to produce a loading similar to the application and removal of load under service conditions.

Strain gauges were located on the top and bottom flanges of each girder at seven sections along the bridge as illustrated in Figure 2. Since these sections were critical in the girders, both strain-gauge locations and section locations were designated in terms of the section numbers and girder numbers shown in Figure 2. A designation of 2.4B means section 2, girder 4 (north exterior girder), bottom flange.

Additional instrumentation included deflection gauges at the centers of all spans, gauges to measure slip between the slab and the girders, and accelerometers at several locations. All strain and deflection gauges were read and recorded automatically either on punched paper tape by using a peak detector and a 100-channel scanner or on magnetic tape by using a high-speed analog-to-digital converter.

Prior to the start of fatigue loading, the bridge was thoroughly inspected for cracks by using all the techniques except dye penetrant. During fatigue loading, the test was stopped periodically for inspection by the various crack-detection techniques. Inspection intervals varied from approximately 20 000 to 60 000 cycles depending on the degree of cracking activity that was occurring at the time. It was possible to conduct visual and some ultrasonic inspection while fatigue loading was being applied, and these observations were used as a guide in selecting the times at which the test should be stopped for complete inspection. A complete description of the test procedure has been presented by Baldwin, Salane, and Duffield (5).

Figure 1. Electrohydraulic shaker.

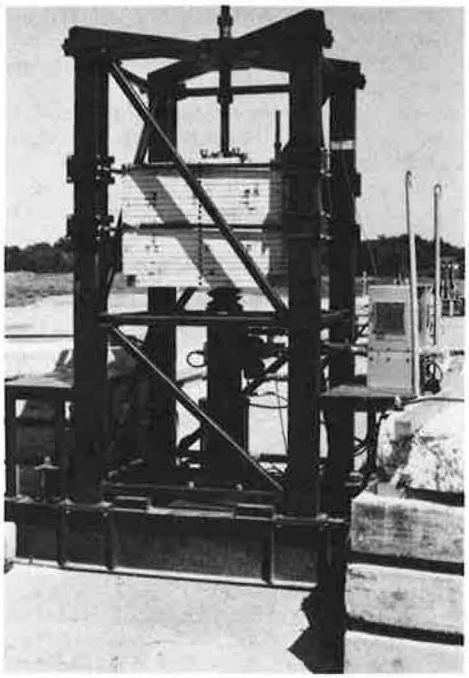

FATIGUE CRACKS

Ultrasonic inspection prior to loading revealed only one detectable flaw, and follow-up inspections during the test indicated that this flaw did not develop into a crack. The feasibility study for the project indicated that the critical regions for fatigue cracking would be at the ends of the bottom-flange cover plates in the end spans, gauge sections 2 and 6.

Bottom-Flange Critical Section

Nominal stresses at these sections, including dead load, ballast, and dynamic load, were from approximately 138 MPa (20 ksi) compression to 17 MPa (2.5 ksi) tension, or a stress range of 155 MPa (22.5 ksi). Variations from girder to girder were approximately ±10 percent from these values.

Figure 2. Strain-gauge locations.

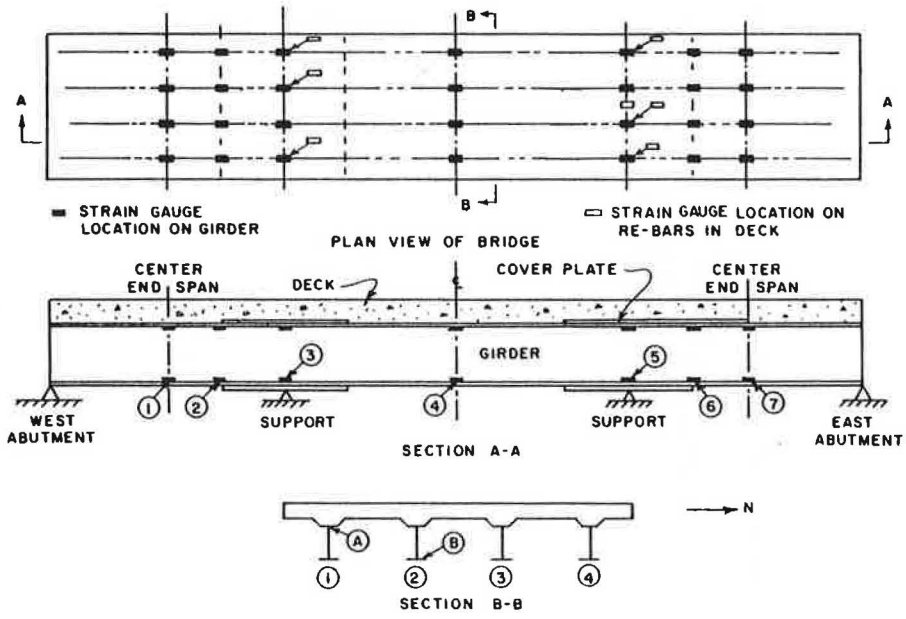

During the inspection at the end of 19 500 cycles of load, cracks of the order of 6.4 mm (0.25 in) length were detected ultrasonically in five of the eight critical flange regions. After 287 000 fatigue cycles, cracks had been detected in all eight of these critical regions. These cracks did not initiate at the toe of the weld as might have been expected but started at the root or heel of the weld at some point across the end of the cover plate as shown in Figure 3. These cracks did not enter the girder flange at this point but propagated along the fusion line to the surface of the weld and across the end of the cover plates. In most cases, they turned the corner of the cover plate and proceeded along the beveled edge until at some point the crack turned into the weld metal propagating perpendicular to the axis of the beam (Figure 4). Once the cracks had entered the weld material, they continued through it into the base metal of the bottom flange and continued to grow in the typical semielliptical pattern. In five of the eight critical flange regions, the cracks propagated into the base metal on both sides of the cover plate, which resulted in two separate cracks in the base metal (Figure 5).

Figure 3. Crack initiation at heel of weld.

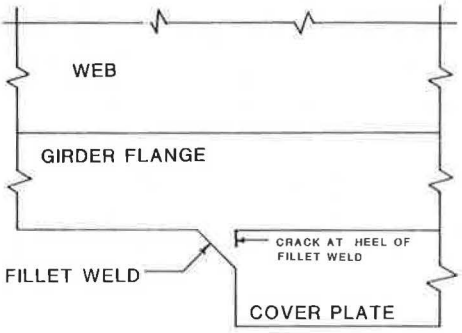

Figure 4. Crack propagation.

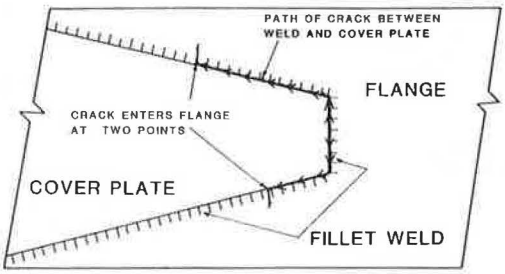

Figure 5. Cross section of flange showing two fatigue cracks.

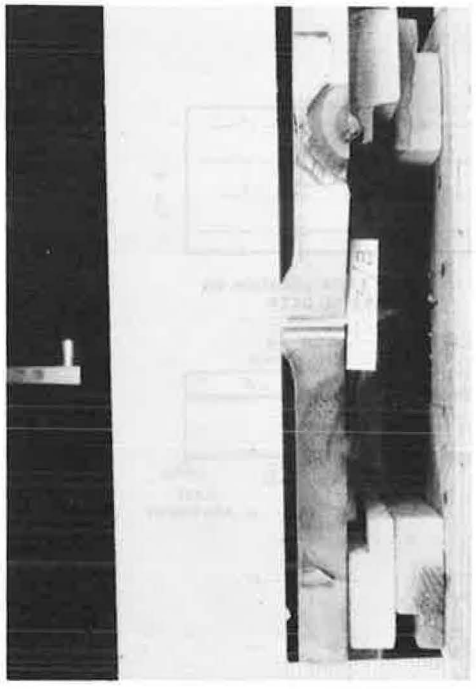

In all there are 13 separate cracks that entered the base material of the bottom flanges at the ends of cover plates. Two of these cracks, located at section 6.1B, propagated to failure and completely severed the bottom flange at 455 000 fatigue cycles. The crack on the south side at section 2.2B propagated to a total length of 90 mm (3.5 in) at 438 000 cycles but showed no perceptible additional growth beyond that point (Figure 5). No growth was observed in any of the other 10 cracks beyond approximately 415 000 fatigue cycles.

In the design of ductile structures subjected to static loads, it is normal practice to consider stresses that result from directly applied loads and neglect "locked-in" stresses such as cooling residual stresses and erection stresses. Under static loading, these locked-in stresses are dissipated by local yielding with very little effect on the general behavior of the structure. Fatigue-crack growth, however, is governed by the actual stress cycles in the zone around the tip of the crack, and locked-in stresses are superimposed on the nominal stress cycle in this zone. Thus the actual stress cycle has the same stress range as the nominal cycle but a significantly different mean stress.

It is reasonable to assume that the test bridge contained tensile residual stresses equal to the yield point in regions of the flanges in which fatigue cracks entered the base metal from the weld. Consideration of these residual stresses results in the stress-cycle pattern shown in Figure 6. Both dead load of the slab and ballast loads produced compression in the bottom-flange critical sections that reduced the total stress at the crack-initiation points from the yield point of 262 MPa (38 ksi) to 202 MPa (29.25 ksi). The cyclic dynamic load was then superimposed on this mean stress and as the amplitude built up to $\pm$77.6 MPa (11.25 ksi), the maximum stress again reached the yield point, which caused local yielding. This yielding relieved part of the residual stress, which in turn lowered the mean stress.

Mean stress at the crack tip then remained constant and maximum stress reached the yield point on each cycle as the crack propagated through the tensile-residual-stress zone. As the crack propagated from the tensile-residual-stress region into the region of zero residual stress, the mean stress decreased to -60 MPa (-8.75 ksi), the sum of dead load and ballast stresses.

A total of 13 cracks propagated in the tensile-residual-stress zones where the mean stress was 202 MPa, but even though the stress range remained constant, all except one of these cracks stopped growing when the mean stress dropped to -60 MPa. This suggests that mean stress at the tip of the crack must be significant in at least those cases in which part of the stress cycle is in compression.

This observation is consistent with a fracture-mechanics analysis if it is assumed that fatigue-crack growth is governed primarily by the stress-intensity range ΔK_I. The general form of the equation for computing K_I is as follows:

Figure 6. Fatigue stress cycles.

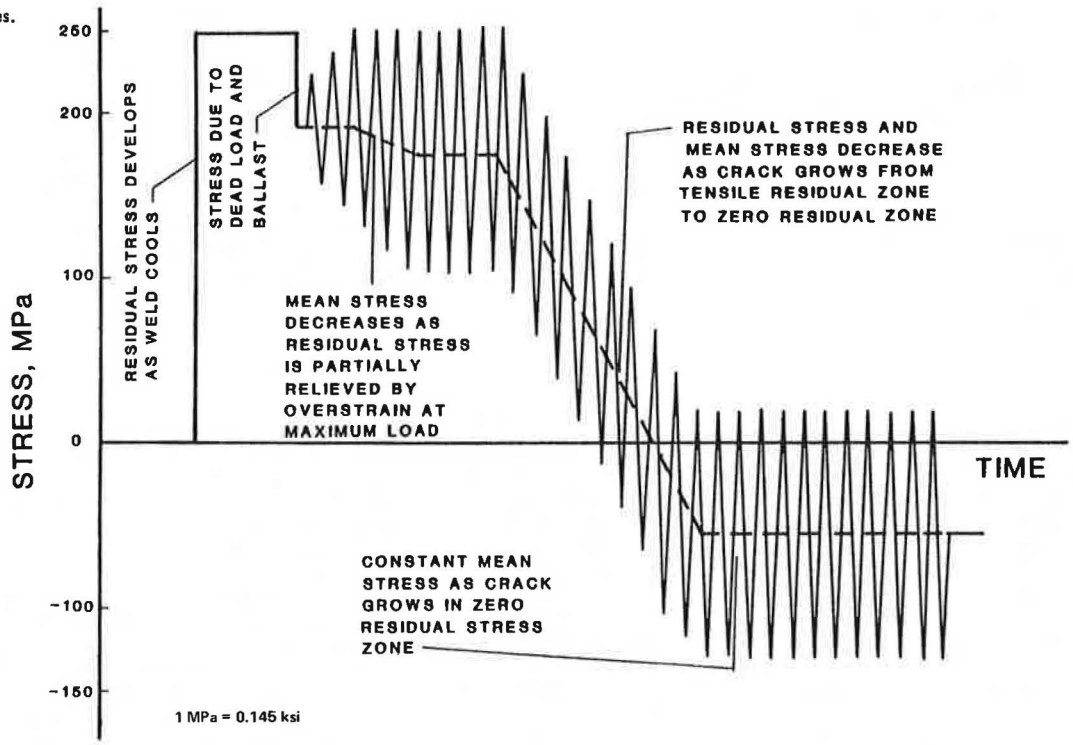

$$K_I = C\sigma\sqrt{a} \quad (1)$$

where C is a constant dependent on the geometry of the member and type of crack, σ is the nominal stress, and a is the crack length. This equation is derived from an elastic analysis of the stress field around the crack tip and is based on the assumption that no stress is transmitted across the crack. As long as the entire stress range in the vicinity of the crack is in tension, the following holds:

$$\Delta K_I = C\Delta\sigma\sqrt{a} \quad (2)$$

and the mean stress does not enter into the analysis. However, if the mean stress is such that compressive stress is transmitted across the crack during part of the cycle, Equation 1 becomes invalid during that part of the cycle. In fact, there is probably very little change in the stress intensity during that part of the cycle when the crack is closed.

The foregoing analysis does not account for the possibility of erection stresses or stresses that arise from differential settlement. Such stresses could be either tensile or compressive, could vary from girder to girder, and are impossible to estimate accurately. If they were tensile, they would cause immediate local yielding and no increase of total stress in regions where initial tensile residual stresses were already to the yield point.

The total stress would remain at the tensile yield point and stress cycles would be unaltered during crack initiation and growth through the tensile-residual-stress zone. Once the crack tip reached the zero-residual-stress region, presence of tensile erection or settlement stress would raise the mean stress above the level shown in Figure 6 by an amount equal to the erection or settlement stress.

Erection or settlement stresses algebraically less than -17 MPa (-2.5 ksi) would lower the entire stress pattern and force the complete stress cycle into the compression zone before the crack tip reached the region of zero residual stress. Stresses of this type could easily account for variations in the lengths at which crack growth was arrested in different sections.

Top-Flange Critical Sections

Calculations during the feasibility study indicated that stress ranges at the ends of the top-flange cover plates in the end spans, gauge sections 2 and 6, would be 90-97 MPa (13-14 ksi) and that there was the possibility of failure before 500 000 cycles. The initial test plan therefore called for continuous ultrasonic monitoring of these regions.

Once the test load was under way, strain measurements indicated that there was considerably more composite action at these critical sections than had been assumed during the feasibility study. Nominal stresses under test loading were from approximately 41 to 101 MPa (6.0-14.7 ksi) tension, which produced an average stress range of only 60 MPa (8.7 ksi). Both the AASHO specifications and previous research results presented by Fisher indicated a fatigue life of nearly 2 million cycles under this low stress range. Because of this and the fact that ultrasonic testing was the critical activity in a very tight testing schedule, ultrasonic monitoring of the top flanges was discontinued.

However, at 415 000 fatigue cycles, a routine visual inspection of the bridge revealed that cracks approximately 150 mm (6 in) long had developed in the top flanges of girder 1 at section 2 and girder 2 at section 6. Ultrasonic monitoring of the top flanges at sections 2 and 6 was immediately reinstated, but no additional cracks in top flanges were detected during the tests. The cracks in girder 1 at section 2 and girder 2 at section 6 propagated to failure, completely severing the flanges at 453 000 and 462 000 cycles, respectively. After completion of the fatigue test, the slab was removed and cracks in the welds at the ends of the cover plates were detected by using dye penetrant at sections 2.1A, 2.3A, and 6.1A.

The fact that two of the eight sections subjected

Figure 7. Detail of top-flange critical section.

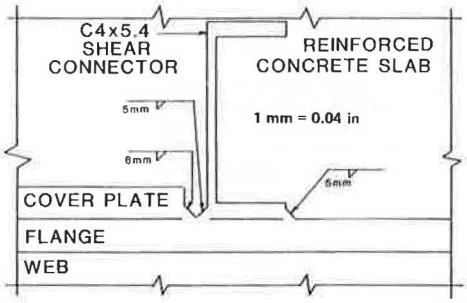

to essentially the same loading failed at less than 25 percent of the cycles permitted by the current code is reason for concern. In addition to the magnitude of stress range, there were two primary differences between these top-flange critical sections and the bottom flanges immediately below them. In the top flanges, the nominal stress range was entirely in the tension region; the maximum tensile stress was 101 MPa (14.7 ksi), whereas the nominal stress range in the bottom flanges was primarily in the compression region and the maximum tensile stress was only 17 MPa (2.5 ksi). The other difference was the particularly severe weld detail in the top flange. A channel shear connector had been fillet-welded to the base metal of the top flange adjacent to the end of the cover plate so that the two fillet welds were toe to toe and slightly overlapped (Figure 7).

In the vicinity of the welds where the cracks began, any effect of the difference in maximum nominal stresses between the top and bottom flanges would have been negated by the fact that tensile residual stresses would have raised the maximum stress at the crack tip to the yield point in both cases. Thus, any differences in crack initiation between the top and bottom flanges must have been due to differences in stress range and detail. It is clear that the stress range in the top flange was not great enough to initiate cracks in the same way that they were initiated in the bottom flanges. The five cracks that did begin in the top flanges all started at the intersection of the two fillet welds. The fact that two of the cracks started much earlier than the other three and that there were three top flanges in which no cracks were detected suggests that there were significant differences in the severities of flaws in these regions. At section 6.2A there was a 5-mm (0.19-in) slag inclusion that apparently initiated the crack. Unfortunately, the nearly two years that elapsed between the end of the fatigue test and demolition of the bridge deck permitted severe corrosion of the fracture surfaces, and attempts to identify the point of crack initiation at section 2.1A were unsuccessful.

Because the only top-flange cracks that grew significantly were quite large before they were detected, it is difficult to draw conclusions regarding the growth rates of these cracks. However, the fatigue lives of the top flanges that did develop cracks early were rather short for the stress range involved. This would have been influenced some by the size of the flaws that initiated the cracks. It was also undoubtedly influenced considerably by the length of the zone of high residual tensile stress. The geometry of the weld detail was such that these cracks would have grown in the zone of high tensile stress in which the maximum stress at the crack tip was equal to the yield point for more than one third of the width of the flange.

At 415 000 fatigue cycles, cracks at sections 6.2A, 2.1A, and 6.1B were all approximately the same length. Even though the stress range at section 6.1B was 2.5 times those at the other two sections, the first failure was 2.1A and all three sections failed within a 9000-cycle period. During the period from 415 000 cycles to failure, all three cracks were growing in regions of base metal in which there was probably little or no residual stress and little influence from weld details. Thus, the growth rate at section 6.1B must have been retarded by the fact that much of the stress cycle was in compression.

Center Span

At 373 500 fatigue cycles, the bottom flange at girder 2 failed with a loud bang at the center of the center span. Although the stress cycles at this section were from essentially nothing to 223 MPa (32.3 ksi), there were no welds on the flange, and base metal at a stress range of 223 MPa would not be expected to fail until more than 1.25 million fatigue cycles had been applied. Examination of the fracture revealed that a fatigue crack had started at a heat number stamped on the face of the bottom flange (Figure 8).

A piece of the beam around the fracture was cut out for laboratory examination and a bolted splice applied so that the test could continue. At 470 700 fatigue cycles, this girder fractured again at another heat number about 102 mm (4 in) from the end of the splice. Although girder 2 suffered two fractures, no cracks were detected in the girders on either side of this girder even though they were both subjected to the same stress conditions and were also heat-stamped on the face of the bottom flange. Girder 2 was from a different heat of steel than the girders on either side, which led to speculation that there was a difference in the fatigue resistance of these two levels of heat. However, subsequent tests of material cut from these three girders have shown no significant differences in material properties. Thus, the difference appears to have been in the sharpness of the heat-stamp dies.

CRACK-DETECTION METHODS

Ultrasonics

During the course of the fatigue test, a total of 17 inspections were conducted by using a conventional pulse-echo ultrasonic unit. For crack detection, the transducer was a 5-MHz 45-degree transceiver probe. For the initial inspection, a 5-MHz 90-degree split-crystal probe was also used to locate the channel shear connectors, which were welded to the top of the top flange and embedded in the slab.

The initial inspection was conducted before testing started and included complete inspection of both the top and bottom flanges at the ends of the cover plates in both the end and center spans. This initial inspection also included locating and marking the ends of the cover plates and shear connectors on the top flanges. The only flaw detected during this inspection was in the fillet weld at the end of the top-flange cover plate on girder 3 at section 6. However, this flaw did not develop into a crack and there was no noticeable change in the flaw during the entire test.

Because bad weather had forced a very condensed testing schedule and ultrasonic inspection proved to be quite time consuming, subsequent inspections were in general limited to the critical regions of the bottom flanges around the ends of the cover plates in the end spans. The second inspection was con-

Figure 8. Fatigue crack initiated by heat stamp.

ducted after 19 530 fatigue cycles. A total of six cracks each approximately 6.4 mm (0.25 in) long were discovered during this inspection. In every case, the ultrasonics clearly indicated that the crack was not at the toe of the weld, as might be expected, but rather at the heel of the weld.

At 95 000 cycles, a total of 10 cracks had been detected ultrasonically, but it was not until 202 000 fatigue cycles that any of these cracks were seen on the surface. Even then they could be seen only with the aid of a dye penetrant. Visual observations by using dye penetrant indicated that in some cases the crack in the weld was considerably longer than indicated by the ultrasonic measurement. This was due at least in part to the fact that without special techniques there is an ultrasonic blind spot directly below the web of the beam. In many cases in which two cracks were recorded, one on either side of the web, they were actually connected through this blind spot and formed a single crack.

All these cracks were monitored for the remainder of the test, and a complete record of crack lengths as measured ultrasonically is presented in Table 1. In those cases in which the cracks propagated across the entire width of the flange, it was possible to trace their growth ultrasonically to within approximately 2.5 mm (0.1 in) of the edge before the crack became visible on the edge.

After completion of the test, two sections that each contained two cracks that had stopped during the test were cut from the bridge and separated in the laboratory. It was then possible to compare the actual lengths of these four cracks with the lengths indicated by ultrasonic measurements. For two of the cracks the ultrasonic measurements were essentially correct. One ultrasonic measurement was in error by 6.4 mm (0.25 in) and the other by 10 mm (0.4 in).

For the critical regions at the ends of the cover plates on the bottom flanges, the conventional pulse-echo ultrasonic unit proved to be quite reliable in finding fatigue cracks under field conditions. All cracks that grew large enough to be detected visually had previously been detected ultrasonically when they were less than 38 mm (1.5 in) long and 60 percent of them were detected at a length of 6.4 mm.

Ultrasonic inspection of the critical regions at the ends of cover plates on the top flanges was not so successful. Because stress ranges were low in the top flanges, ultrasonic inspection was discontinued early in the test and was not resumed until two cracks had been observed visually. Of course, the failure to detect these two cracks ultrasonically cannot be interpreted as an adverse reflection on the capability of the ultrasonic inspection because no attempt was made to detect them. However, subsequent ultrasonic inspections of the other six critical top-flange regions that were subjected to essentially the same stress histories revealed no additional cracking. The cracks that were detected by using dye penetrant subsequent to removal of the deck were missed completely by the ultrasonic inspection. Examination of the geometry of the detail at this joint indicates that it is very difficult to detect cracking at the toe of the fillet weld, as shown in Figure 9. Under ideal conditions the surface of a crack is sometimes rough enough to reflect a signal directly back to the transducer even though the angle of incidence is other than zero, but under field conditions in which the transducer must be acoustically coupled through a painted surface that tends to be rough or irregular, it is almost essential that the signal be reflected either by a surface perpendicular to the ultrasonic beam or by doubling a corner if it is to be strong enough for detection. Thus, there is serious doubt about the reliability of conventional ultrasonic inspection to detect cracks in a detail of this type.

Two undetected cracks developed and grew to complete failure in girder 2 near the center line of the bridge. Since cracking was not expected in this region, there had been no ultrasonic inspection prior to development of the first crack. Immediately after the first crack developed, the entire area was scanned ultrasonically but no additional cracks were detected. Although there was frequent monitoring of this region during the remaining 93 000 cycles of the test, no additional cracks were detected ultrasonically and the final failure was by sudden fracture of girder 2 approximately 1 m (3 ft) from the first fracture. The cracks leading to both these fractures had initiated at heat numbers stamped into the flange. After the test loading had been stopped, these regions were again examined very carefully by using the ultrasonic probe, but no cracks were detected.

Dye Penetrant

Once the ultrasonic inspection indicated that cracks in the weld were 12.7 mm (0.5 in) or more in length, repeated attempts were made to observe these cracks visually at the surface. When these attempts failed, a dye penetrant was introduced to enhance the visibility of the cracks. These attempts were also unsuccessful until the paint was removed from the area to be inspected. However, once the surface was free of paint, the dye penetrant gave a vivid indication of cracks that were previously invisible to the unaided eye. By reapplying the dye penetrant periodically, it was quite easy to trace the progress of crack growth during the remainder of the test.

Since dye penetrant is quite easy to apply and interpretation of the results requires no special training or skill, it would seem to be an excellent field-inspection tool. However, for routine bridge inspection, the removal of paint in all the areas to be inspected would be both difficult and expensive. It is quite likely that once the cracks open up enough to crack the paint, the dye penetrant could be used without removal of the paint. During this test, the paint was removed from all areas soon after the cracks had been detected ultrasonically, and no data were recorded that would indicate how large the crack in the base metal must be before it penetrates the paint layer.

Table 1. Ultrasonic crack measurements in bottom flange.

Inspection No.	Cycles (000s)	Crack Length at Indicated Section (mm)															
		2.1B		2.2B		2.3B		2.4B		6.1B		6.2B		6.3B		6.4B	
		N	S	N	S	N	S	N	S	N	S	N	S	N	S	N	S
1	0																
2	19.5							6[a]		5[a]			6[a]		6[a]	6[a]	6[a]
3	75.4							13[a]							13[a]	10[a]	13[a]
4	95.1	6[a]				6[a]		13[a]	6[a]	6[a]	6[a]		6[a]		13[a]	19[a]	18[a]
5	215.4	6[a]				6[a]		25[a]	6[a]	6[a]	6[a]		6[a]		13[a]	23[a]	25[a]
6	287.0	32[a]		33[a]	25	32[a]	38[a]	38[a]	38[a]	38[a]	38[a]	38[a]	38[a]	33[a]	38[a]	38[a]	25[a]
								6		20	15		27				
7	337.5	38[a]	38[a]	38[a]	38	38[a]	38[a]	38[a]	38[a]	47	46	14	27	38[a]	38[a]		38[a]
		18						6	6						6		6
8	348.7			38[a]						52	51		30				
9	360.9	22		6	38	38[a]	6	18	6	65	58	19	34	6	6		6
10	380.0	22		11	48					69	58	19	37				
11	402.1	22		15	53	38[a]	6	18	6	74	66	20	41	38	6		6
12	415.5	22		15	71	38[a]	6	18	6	85	83	20	44	38	6		6
13	422.5				71					89	83						
14	437.8				89												
15	447.9									119	108						
16	455.0				89					Failure							

Note: 1 mm = 0.0394 in; N = north side of flange; S = south side of flange.
[a]Crack between weld and end of plate; all other measurements are for cracks in base metal of girder flange.

Figure 9. Ultrasonic inspection of top flange.

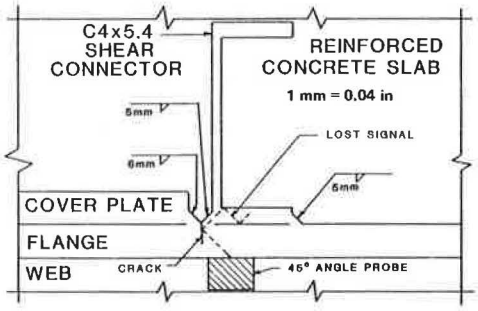

Radiography

Four sets of radiographs were taken by a commercial testing laboratory at 0, 95 000, 215 000, and 377 000 cycles of load. A set of radiographs included one 178x432-mm (7x17-in) film on each side of the bottom flange of each girder at sections 2 and 6. At 0 and 95 000 cycles, the set also included an identical series for the top flanges at sections 2 and 6. Of course, it was necessary to expose films of the top flanges through the reinforced concrete deck slab 152 mm (6 in) thick, and after two attempts it was concluded that interference from aggregate particles and reinforcing bars in the slab would obscure and prevent detection of any cracks that might be present in the top flange. Radiographs of the top flanges were discontinued after the second set. At 377 000 cycles, three additional films were shot along each side of each bottom flange at the center line of span 2.

All exposures were made with a 90-curie source of iridium 192 at a distance of 406 mm (16 in). Exposure times for the bottom flanges were 30 s and those for the top flanges were 15 min.

At 95 000 cycles, no cracks were indicated on the radiographic examination report, whereas the ultrasonic inspection indicated 10 cracks that varied from 6.4 to 19 mm (0.25 to 0.75 in) in length. At 215 000 cycles, the radiographic examination report indicated five cracks across the ends of the cover plates at the heel of the weld, whereas the ultrasonic inspection still indicated 10 cracks, two of which were 25 mm (1 in) long. However, four of the cracks that were detected radiographically were indicated to be only 6.4 mm (0.25 in) long by the ultrasonic inspection and had shown no growth since the previous ultrasonic inspection. The fifth crack had not been detected ultrasonically, and the radiograph showed that it had already penetrated the base metal of the bottom flange.

At 377 000 cycles, the radiographic examination report indicated 12 cracks in the critical regions of the bottom flanges, whereas the ultrasonic inspection indicated a total of 16 cracks. Again, there was no general trend in comparing the crack lengths as indicated by the two methods. For some cracks, the radiograph indicated the greater length, whereas for others the ultrasonic inspection indicated the greater length. The largest crack, which had been observed both ultrasonically and visually with the aid of a dye penetrant to be in excess of 64 mm in length, was not detected radiographically.

The special films exposed in the center span covered a region of the bottom flanges approximately 610 mm (2 ft) on either side of the center line of the bridge. No cracks were detected other than the one complete fracture of girder 2. Unfortunately, the region covered by these films was not quite long enough to cover the section in which the final fracture occurred approximately 93 000 cycles after these films had been exposed.

Radiographic inspection suffers from some of the same shortcomings that affect ultrasonic inspection. There tends to be a blind spot in the center of the flange directly opposite the web. It is also much easier to detect cracks that are oriented along a line from the film to the radiation source. This is because detection depends on the existence of a significant reduction in the density of material along the radiation line through the flange at the location of the crack. Thus, if the crack is not colinear with the radiation, the line intersects the crack for only a short length and there is little change in the total density of material along the line. Cracks can be detected only if they are open at the time the radiograph is taken.

Randomdec

The Randomdec technique of analyzing high-frequency

vibration signatures was employed as an inspection method by instrumenting the bridge with accelerometers at 24 stations. These stations were at the ends of the cover plates located on the top and bottom flanges of the girders in the two end spans. Two accelerometer stations were positioned in each bottom-flange region and one accelerometer station was positioned in each top-flange region. Detailed results of the Randomdec analysis are presented in a report by Reed and Cole (6).

CONCLUSIONS

Fatigue

Crack initiation, crack growth, and fracture are distinctly different phases of fatigue failure, and a given set of conditions may have significantly different effects on the initiation and growth phases. Thus it may not be possible to predict total fatigue life accurately on the basis of a simple relationship that involves only stress range and type of detail.

Both the initiation and growth phases are governed by the nature of stress cycles in a small zone around the tip of the crack. Mean stress in this zone has a significant effect on crack growth and possibly crack initiation, at least in those cases in which part of the stress cycle is in compression. These effects tend to be masked by high levels of tensile residual stress in tests of weldment details. Of course, these residual stresses are also present in prototype structures fabricated according to current practice, but the proportion of the cross section subjected to tensile stress is an important parameter, which may vary considerably from one structure to another. Finally, an understanding of the basic mechanisms of fatigue-crack initiation and growth may suggest changes in current practice that will improve the fatigue resistance of future structures. Additional research is needed to determine the exact stress conditions under which fatigue cracks begin as well as the conditions under which they propagate.

The premature failure of girder 2 at midspan points out the potential for fatigue-crack initiation resulting from the stamping of heat numbers in the flanges. Although this practice has been largely discontinued for rolled sections, it is still common practice to stamp identification numbers in plates during fabrication. If the final location of a stamped identification number is one of high repeated tensile stress, there is certainly a potential for fatigue-crack initiation. Consideration should be given to controlling the use of such identification stamps. The depth and sharpness of the stamp as well as its location are important factors.

Crack Detection

A conventional pulse-echo ultrasonic unit was the most reliable of the inspection methods. In those regions that were monitored regularly, no cracks are known to have grown to a length greater than 38 mm (1.5 in) without ultrasonic detection. However, undetected cracks did develop in regions that were not being monitored, and there is serious doubt whether those cracks would have been detected ultrasonically even if the region had been monitored.

Visual inspection appeared to be the second most reliable method of detection. Of course, cracks must penetrate the observed surface in order to be detected visually. Use of a dye penetrant significantly reduced the size of crack that could be detected visually.

Radiography was nearly as reliable as ultrasonic inspection in the regions in which it could be used. However, more than half the material to be inspected was inaccessible to radiography.

In some of the critical fatigue zones, the Randomdec method of detecting cracks produced crack predictions consistent with the ultrasonic results. However, the findings indicate that the methods of excitation employed in this study to generate the vibration signatures needed for the Randomdec analysis are not completely adequate for reliable crack detection.

The reliability of conventional ultrasonic techniques and radiography is sufficient to warrant the continued development of inspection programs that use these techniques along with visual inspection. However, it must be recognized that in the vicinity of complex connections, some cracks may become very large before they can be detected.

ACKNOWLEDGMENT

Research reported here was sponsored by the Missouri Highway Commission and the FHWA as a Highway Planning and Research Study. The bridge was made available by the U.S. Army Corps of Engineers, Memphis District. We gratefully acknowledge the help of numerous members of the Missouri Highway Department, FHWA, and Army Corps of Engineers. Robert E. Reed of Nielsen Engineering and Research, Inc., conducted the Randomdec study. Stanley T. Samborski III, former research assistant in civil engineering, is due special recognition for his work in collecting and reporting of the ultrasonic inspection and fatigue data.

REFERENCES

1. J.W. Fisher, K.H. Frank, M.A. Hirt, and B.M. McNamee. Effect of Weldments on the Fatigue Strength of Steel Beams. NCHRP, Rept. 102, 1970.
2. J.W. Fisher, P.A. Albrecht, B.T. Yen, D.J. Klingerman, and B.M. McNamee. Fatigue Strength of Steel Beams. NCHRP, Rept. 147, 1974.
3. Standard Specifications for Highway Bridges, 8th ed. American Association of State Highway Officials, Washington, DC, 1961.
4. H.J. Salane, R.C. Duffield, R.P. McBean, J.W. Baldwin, and T.V. Galambos. An Investigation of the Behavior of a Three-Span Composite Highway Bridge. Missouri Cooperative Highway Research Program, Rept. 71-5, Nov. 1971.
5. J.W. Baldwin, H.J. Salane, and R.C. Duffield. Fatigue Test of a Three-Span Composite Highway Bridge. Missouri Cooperative Highway Research Program, Rept. 73-1, June 1978.
6. R.E. Reed, Jr., and H.A. Cole, Jr. Randomdec: Mathematic Background and Application to Detection of Structural Deterioration in Bridges. FHWA, Rept. FHWA-RD-76-181, 1976.

Publication of this paper sponsored by Committee on Dynamics and Field Testing of Bridges.